

1 **23 January 2023** Revised Submittal for *Earth and Space Science*

2 **Two Air Quality Regimes in Total Column NO₂ over the Gulf of Mexico in May 2019: Shipboard**
3 **and Satellite Views**

4
5 Anne M. Thompson^{1,2}, Debra E. Kollonige^{1,3}, Ryan M. Stauffer¹, Alexander E. Kotsakis^{1,4}, Nader
6 Abuhassan^{1,2}, Lok N. Lamsal^{1,2}, Robert J. Swap¹, Donald R. Blake⁵, Amy Townsend-Small⁶, Holli D.
7 Wecht⁷

8
9 ¹Earth Sciences Div., NASA/Goddard Space Flight Center, Greenbelt, MD 20771;

10 anne.m.thompson@nasa.gov Orcid: 0000-0002-7829-0920; ryan.m.stauffer@nasa.gov Orcid: 0000-
11 0002-8583-7795

12 ²Univ. Maryland-Baltimore County, GESTAR and Joint Center for Earth Systems Technology, Baltimore,
13 MD 21228;

14 ³SSAI, Lanham, MD 20706 debra.e.kollonige@nasa.gov Orcid: 0000-0002-6597-328X

15 ⁴ERT, Inc., Laurel, MD 20707; alexander.e.kotsakis@nasa.gov

16 ⁵Univ. California-Irvine, Dept. of Chemistry, Irvine, CA 92697, drblake@uci.edu;

17 ⁶Univ. of Cincinnati, Dept. of Geology and Geography, Cincinnati, OH 45221-0091;

18 townseay@ucmail.uc.edu

19 ⁷Bureau of Ocean Energy Management, Office of Environmental Programs, Sterling, VA 20166;

20 holli.wecht@boem.gov

21

22 Three points-

- 23 ■ Shipboard Pandora NO₂ columns and surface O₃, NO₂, CO and VOC over the Gulf of Mexico,
24 May 2019, displayed two air quality (AQ) regimes
25 ■ Gulf of Mexico (GOM) AQ was dominated by continental NO₂ sources and near-shore VOC;
26 deepwater oil platforms were in a clean marine regime
27 ■ Pandora and satellite total column NO₂ over GOM agreed overall within 5% in clean, clear-sky
28 conditions at the coast and 13% over water

29

30 Keywords: Pandora spectrometer, Pollution – Energy Sector, Gulf of Mexico, OMI NO₂

31 Index Terms: 0345, 0365, 1610, 1640

32 **ABSTRACT.**

33 **Abstract.** The Satellite Coastal and Oceanic Atmospheric Pollution Experiment (SCOAPE)
34 cruise in the Gulf of Mexico was conducted in May 2019 by NASA and the Bureau of Ocean
35 Energy Management to determine the feasibility of using satellite data to measure air quality in a
36 region of concentrated oil and natural gas (ONG) operations. SCOAPE addressed both
37 technological and scientific issues related to measuring NO₂ columns over the Outer Continental
38 Shelf. Featured were nitrogen dioxide (NO₂) instruments (Pandora, Teledyne API analyzer) at
39 Cocodrie, LA (29.26°, -90.66°), and on the *Research Vessel Point Sur* operating off the Louisiana
40 coast with measurements of ozone, carbon monoxide and volatile organic compounds (VOC). The
41 findings: (1) All NO₂ observations revealed two atmospheric regimes over the Gulf, the first
42 influenced by tropical air in 10-14 May, the second influenced by flow from urban areas on 15-17
43 May; (2) Comparisons of OMI v4 and TROPOMI v1.3 TC (total column) NO₂ data with
44 shipboard Pandora NO₂ column observations averaged 13% agreement with the largest difference
45 during 15-17 May (~20%). At Cocodrie, the satellite-Pandora agreement was ~5%. (3) Three new-
46 model Pandora instruments displayed a TC NO₂ precision of 0.01 Dobson Units (~5%); (4)
47 Regions of smaller, older natural gas operations showed high methane readings from leakage;
48 elevated VOC were also detected. Neither satellite nor spectrometer captured the magnitude of
49 ambient NO₂ variability near ONG platforms. Given an absence of regular air quality monitoring
50 over the Gulf of Mexico, SCOAPE data constitute a baseline against which future observations
51 can be compared.

52 **Plain Language Summary.** The Satellite Coastal and Oceanic Atmospheric Pollution
53 Experiment (SCOAPE) cruise in the Gulf of Mexico (GOM) conducted on the *Research Vessel*
54 *Point Sur* in May 2019 investigated the feasibility of using satellite data to measure air quality in a
55 region of concentrated oil and natural gas (ONG) operations. SCOAPE addressed both
56 technological and scientific issues related to measuring NO₂ columns in a prototypical coastal
57 environment. The results are as follows. First, measurements from SCOAPE demonstrated that
58 satellite NO₂ data *can* be used to monitor ONG activity over the GOM. Second, during SCOAPE
59 both OMI and TROPOMI TC (total column) NO₂ amounts were higher over land and sometimes
60 the near-shore ONG-rich Gulf, than over deepwater regions farther offshore. This was confirmed
61 by Pandora spectrometer “ground truth” TC NO₂ data measured throughout SCOAPE on shore
62 and on ship. Third, SCOAPE established the reliability and precision of a new generation of
63 Pandora spectrometers. Fourth, comparisons of satellite and Pandora TC NO₂ data in SCOAPE
64 confirm previous land-water interface studies that point to limitations in satellite NO₂ in coastal
65 regions. Finally, neither satellite nor spectrometer captures the magnitude of ambient NO₂
66 variability in a region dotted with hundreds of ONG platforms.

67 1. Introduction

68 1.1 Background

69 Within the past decade, there have been several focused studies of air quality (AQ) along North
70 American coastlines where pollutants display distinct air-water gradients due to interactions of
71 complex marine meteorology with rapidly reacting chemical constituents. Because satellite data
72 are viewed as fundamental to large-regional AQ observations, the sampling strategies of these
73 campaigns include space-borne sensors that may be tested to the limit in terms of detection
74 thresholds, accuracy and precision. Experimental designs complement the satellite observations
75 with airborne, ship and ground-based instruments that may themselves be using technology in
76 development. Measurements from these experiments are typically used in comparisons with
77

78 satellite column amounts and, in some cases, can be used to improve the satellite retrievals.
79 Nitrogen dioxide (NO₂) is an important constituent for remote sensing measurements because
80 NO₂ can be used as a proxy for nitrogen oxides (NO_x = nitric oxide (NO) + NO₂), a product of
81 combustion and a major precursor for the formation of ozone.

82 Satellite, airborne and ground-based instruments for the remote sensing of NO₂ have been
83 employed for decades. For example, satellites have been measuring NO₂ since the mid-1990s,
84 starting with the GOME series (*Burrows et al.*, 1999). These and other long-term records, e.g.
85 from Aura's OMI (Ozone Measuring Instrument), are well-known for characterizing global,
86 regional and temporal variability (*Duncan et al.*, 2013; 2016; *Levelt et al.*, 2018). Seasonal
87 patterns and trends in NO₂ as well as signatures of extreme events, e.g., the 2008-2010 recession,
88 the 2020 COVID-19 pandemic, are well-documented (*Russell et al.*, 2012; *Tong et al.*, 2015;
89 *Goldberg et al.*, 2020). Airborne instrumentation used to measure column amounts and profiles of
90 NO₂ includes DOAS (*Heue et al.*, 2008; *Tack et al.*, 2019) and NASA's GEO-TASO (*Nowlan et*
91 *al.*, 2016) and GCAS (*Judd et al.*, 2020).

92

93 1.2 Remote Sensing Studies of Coastal Air Quality/Overview of Recent Results

94 A host of ground-based UltraViolet (UV)/Visible NO₂ instruments were intercompared in the
95 Cabauw Intercomparison Campaign of Nitrogen Dioxide measuring Instruments (CINDI)
96 campaigns (*Piters et al.*, 2012; *Tirpitz et al.*, 2021) and the 2019 TROPomi vaLIdation
97 eXperiment (TROLIX; *Kreher et al.*, 2020). The Pandora spectrometer is a relatively new ground-
98 based spectrometer (*Herman et al.*, 2009; *Herman et al.*, 2018) that has been used to measure
99 column NO₂ in several coastal experiments: CAPABLE (*Knepp et al.* 2015) in 2010-2011;
100 DISCOVER-AQ in Maryland in July 2011 (*Reed et al.*, 2015; *Tzortziou et al.*, 2015a);
101 DISCOVER-AQ in Houston in 2013 (*Judd et al.*, 2019); DANCE in 2014 off the Virginia and
102 North Carolina coast (*Martins et al.*, 2016; *Kollonige et al.*, 2018); KORUS-OC in 2016 around
103 the Korean peninsula (*Tzortziou et al.*, 2015b; *Tzortziou et al.*, 2018; *Thompson et al.*, 2019a),
104 OWLETS-1 in 2017 in the lower Chesapeake Bay (*Sullivan et al.*, 2018; *Gronoff et al.*, 2019),
105 OWLETS-2 in 2018 in the upper Chesapeake Bay (*Sullivan et al.*, 2020; *Kotsakis et al.*, 2022) ,
106 LMOS in 2017 (*Stanier et al.*, 2021) and LISTOS (Long Island Sound) in 2018 (*Judd et al.*, 2020;
107 *Karambelas*, 2020). **Table 1** gives a list of campaigns and experiments that preceded SCOAPE. A
108 summary of findings from these studies:

- 109 • Agreement between the sun-tracking Pandora and satellite TC NO₂ with satellite varies
110 depending on viewing geometry (*Verhoelst et al.*, 2021). The satellite footprint size at nadir is
111 ~13x24 km for OMI and 3.5 x 7.2 km for TROPOMI during field campaigns in 2018 through
112 July 2019. In general, agreement of Pandora TC NO₂ is closer to TROPOMI than for OMI,
113 especially if the larger satellite pixel includes considerable spatial heterogeneity (*Thompson*,
114 2020; *Thompson et al.*, 2020).
- 115 • At very polluted locations, as TC NO₂ measured from the surface increases, there tends to
116 be greater disagreement with the corresponding satellite TC NO₂. (*Herman et al.*, 2019). This
117 can be due to the heterogeneity of a region Pandora senses as polluted.
- 118 • Besides comparing NO₂ column amounts from satellite or another instrument to the
119 Pandora, the relationship between continuous surface NO₂ and Pandora TC NO₂ in coastal
120 environments has been investigated (*Knepp et al.*, 2015; *Martins et al.*, 2016; *Kollonige et*
121 *al.*, 2018; *Thompson et al.*, 2019a). Correlations between time-coincident surface NO₂ and
122 Pandora TC NO₂ vary considerably. Causes of the divergence may be meteorological, for
123 example, when the Pandora senses an NO₂-rich residual layer located above a relatively
124 unpolluted boundary layer (*Kotsakis et al.*, 2022). Cloud interferences in remotely sensed

125 columns tend to be important along coastlines. In shipboard experiments, the in-situ
126 instrument may be detecting plumes that are not in the field of view of the Pandora
127 (*Thompson et al.*, 2019a).
128

129 **1.3 SCOAPE Background and Scientific Issues**

130 None of the experiments described in **Table 1** were based on comprehensive air quality
131 measurements over a major body of water. The Satellite Coastal and Oceanic Atmospheric
132 Pollution Experiment (SCOAPE) cruise, designed by NASA's Goddard Space Flight Center
133 (GSFC) and the Department of the Interior's Bureau of Ocean Energy Management (BOEM),
134 offered an opportunity to study NO₂ pollution over the Gulf of Mexico (GOM). BOEM issues
135 leases for oil and natural gas (ONG) exploration in the outer continental shelf (OCS; 3-200 nm
136 [5.4-370 km] off Louisiana and Alabama) of the GOM and has jurisdiction over air quality west of
137 87.5°W. Based on fuel usage reported by energy, shipping and other industries over the central and
138 western GOM, BOEM compiles estimates for NO₂, SO₂ and VOC emissions in the region (*Wilson*
139 *et al.*, 2017; 2019). However, there are no air quality monitors over the GOM. In the past decade
140 NASA has refined OMI and other satellite products aimed at regional air quality (e.g., *Boersma et*
141 *al.*, 2018; *Lamsal et al.*, 2014; *Lamsal et al.*, 2017; *Lamsal et al.*, 2021). TROPOMI NO₂ products
142 have been reported by *Goldberg et al.* (2021). At the same time, since 2018 upgraded models of
143 the Pandora instrument (*Robinson et al.*, 2020; *Spinei et al.*, 2021; *Kotsakis et al.*, 2022) have been
144 deployed to evaluate OMI and TROPOMI satellite products.

145 The SCOAPE campaign collected GOM pollution data for the first time while advancing both
146 satellite and Pandora capabilities. A ship cruise was designed for assessing satellite capability for
147 the measurement of trace species required to characterize GOM air quality off the eastern
148 Louisiana coast where oil and natural gas exploration, extraction and production activities are
149 heavily concentrated. In addition to BOEM's emissions database, meteorological and logistical
150 considerations (avoiding winter storms, late summer hurricanes) determined the sampling strategy.
151 Onshore flow was desired to be able to detect air masses arriving from the Gulf. Because both
152 satellite and the Pandora spectrometer operate in the near UV-Visible region, minimizing cloud
153 cover was a criterion for logistics. May 2019 was selected; climatology shows less cloudiness and
154 more onshore flow in May than in June or July.

155 The SCOAPE cruise was planned to address the following questions:

- 156 1. What do pollutant levels measured by satellite over the GOM look like, and how do
157 deepwater regions compare to coastal Louisiana? What role does meteorology play in any
158 observed differences? *Both satellite and shipboard measurements of total column (TC)*
159 *NO₂ are used to address this question.*
- 160 2. Can satellite observations detect emissions from ONG operations over the GOM and are
161 the measurements accurate? *This is addressed by comparing TC NO₂ from satellite*
162 *overpasses over the GOM with TC NO₂ from Pandora over both land and ocean.*
- 163 3. How accurately do Pandora NO₂ measurements track day-to-day variations in emissions?
164 How precise are Pandora TC NO₂ observations? *Pandora data are compared to shipboard*
165 *NO₂ concentrations in the vicinity of ONG operations. Precision is addressed by deploying*
166 *three Pandoras together 4 weeks in advance of the cruise.*
- 167 4. Is there a difference in pollutant emissions between large, deepwater ONG platforms and
168 the hundreds of small near-shore operations? *Whole-air samples collected near platforms*
169 *are analyzed for VOC and other chemical tracers.*

170

171 **Section 2** describes the design of the SCOAPE cruise, instrumentation and ancillary data used
172 for analysis. **Section 3** presents results with interpretation and discussion. It turns out that the
173 cruise period was characterized by two distinct meteorological regimes (**Section 3.1**) that were
174 reflected in contrasting chemical composition over the GOM. Details of these regimes in terms of
175 satellite and shipboard NO₂ measurements, as well as data from other pollution tracers, appear in
176 **Sections 3.2 and 3.3. Section 4** is a summary.

178 **2. Experimental: Cruise Design, Operations, Instrumentation, Ancillary Data and** 179 **Analysis**

180 The cruise track for the *Research Vessel [R/V] Point Sur* is superimposed on the Google Earth
181 Map (**Figure 1**) with land and major platform locations and color-coded NO_x emissions (*Wilson et*
182 *al.*, 2019). In addition to the LOOP (Louisiana Offshore Oil Port, an exclusion zone for research
183 operations) and heavy commercial ship traffic – fishing, energy- and non-energy-related -- there
184 are two basic types of ONG operations in the GOM. Deep-water platforms, typically the largest
185 and located farther from shore, are the most polluting individual operations, corresponding to
186 locations color-coded yellow-orange-red in **Figure 1**; they primarily produce oil with
187 accompanying natural gas flared off. Closer to shore are hundreds of older, small operations in
188 higher-density but with less NO_x emitted per platform. Most of those emitters are in blue and light
189 blue in **Figure 1**.

190 The *R/V Point Sur* departed LUMCON (Louisiana Universities Marine Consortium;
191 <https://lumcon.edu>) Cocodrie, LA, facility (29.26°, -90.66°) at midnight starting 10 May 2019. The
192 ship headed east on entering the GOM, sampling in the eastern region of high-density operations
193 (10-11 May, with the Petronius platform easternmost in **Figure 1**) before heading south and
194 southwest toward deepwater platforms. The 10 May sampling was conducted by automated
195 instruments only; the sea was too rough for deck work. Clouds continued through 12 and 13 May.
196 The southernmost point of the cruise was near the Atlantis platform; legs to the Brutus platform
197 and back to the Atlantis platform followed (13 May in **Figure 1**). Deepwater sampling concluded
198 with a return to Mars/Olympus (14 May), followed by the track east and north toward the
199 Petronius platform (15 May revisit). The *R/V Point Sur* headed toward the higher-density platform
200 region to the west, sampling on 16 May. The cruise finished with a LOOP circumnavigation (17
201 May in **Figure 1**) before returning to LUMCON in the afternoon (local time) of 18 May 2019.

202 **2.1. NO₂ Observations**

203 2.1.1 OMI and TROPOMI

204 We use total column NO₂ observations that are available once-daily from OMI on the NASA
205 Aura satellite (2004 to present) and from ESA's TROPOMI instrument (*Veefkind et al.*, 2012) on
206 the Sentinel-5P satellite (2018-present). Overpasses for both satellites occur early afternoon
207 approximately between 1300-1400 LT. OMI operates with fields of view (FOVs) varying in size
208 from ~13 km x 24 km near nadir to ~24 km x 160 km at the outermost edges of the swath,
209 observing direct and back scattered solar radiation between 264-504 nm needed for retrieving NO₂
210 column (total, tropospheric, and stratospheric) densities (*Levelt et al.*, 2006; *Boersma et al.*, 2011;
211 *Levelt et al.*, 2018). NASA OMI NO₂ Standard Product, V3.1 (OMNO2 product; *Krotkov et al.*,
212 2017), validated in *Choi et al.* (2020), was available for preliminary reports on SCOAPE
213 (*Thompson, 2020; Thompson et al.*, 2020). The current analysis uses the new OMI V4.0 OMNO2
214 data described in detail in *Lamsal et al.* (2021). Differences between V3.1 and V4.0 OMI NO₂
215 data include significant improvements in air mass factors (AMFs), crucial for calculating vertical
216 column NO₂ from slant column amounts, via a new surface reflectivity product and cloud

217 retrievals for NO₂. Specifically, the V4.0 algorithm now incorporates: (1) a new daily and OMI
218 field of view specific geometry-dependent surface Lambertian Equivalent Reflectivity (GLER)
219 product in both NO₂ and cloud retrievals; (2) improved cloud parameters from a new cloud
220 algorithm (OMCDO2N) that are retrieved consistently with NO₂; and (3) a more accurate terrain
221 pressure calculated using OMI ground pixel-averaged terrain height and monthly mean Global
222 Modeling Initiative (GMI) terrain pressure. This product contains total, stratospheric, and
223 tropospheric NO₂ vertical column densities (VCDs) and is available at:
224 https://disc.gsfc.nasa.gov/datasets/OMNO2_V003/summary/. Both V3.1 and V4.0 versions of
225 OMI NO₂ column data are presented in this work using OMI pixels with effective cloud fraction
226 (ECF) less than 30% and quality flags indicating good data for comparisons in the GOM land-
227 water interface.

228 The TROPOMI NO₂ algorithm (*van Geffen et al.* [2022] and references therein) uses a three-
229 step approach, initially used for the Dutch OMI NO₂ product (DOMINO; *Boersma et al.*, 2007),
230 starting with the Differential Optical Absorption Spectroscopy (DOAS) method that determines
231 the slant column density (SCD) with spectral information from the visible band (400-496 nm) as
232 described by *van Geffen et al.* (2018). Individual TROPOMI NO₂ column ground pixels are 7.2
233 km in the along-track and 3.6 km in the across-track direction at nadir (~ 14 km wide at the edge
234 of swath). The latest TROPOMI NO₂ algorithm improvements are described in *van Geffen et al.*
235 (2022) including differences between v1.3 and the latest v2.1/2.2 data products. During the
236 SCOAPE cruise and the period of the current analysis, only v1.3 offline data were available at the
237 European Space Agency (ESA) public data hub (<https://s5phub.copernicus.eu/>) so those
238 measurements are used in this study. (We were able to compare the Sentinel-5P Product
239 Algorithm Laboratory (S5P-PAL) TROPOMI dataset, which uses a newer NO₂ operational
240 processor (version 2.3.1) with the currently available Level 1B radiances. Differences between the
241 S5P-PAL and v1.3 data over the Gulf of Mexico were typically < 5%). The TROPOMI v1.3 NO₂
242 product includes a combined quality assurance value (qa_value) enabling end users to easily filter
243 data. The recommended qa_value > 0.75 to eliminate cloudy scenes and problematic retrievals
244 was applied to the TROPOMI observations presented below.

245 2.1.2 In-situ Analyzers and the Pandora Spectrometer Instrument (PSI)

246 Surface NO₂ mixing ratios were measured by two Teledyne API T500U Cavity Attenuated
247 Phase Shift (CAPS) NO₂ instruments (*Kebabian et al.*, 2005). For a month prior to the cruise as
248 well as during the cruise, one CAPS instrument was situated at the LUMCON building as a
249 reference for the three Pandora spectrometers being tested on the roof. The second CAPS
250 instrument was installed in the portable climate-controlled trailer on the *R/V Point Sur* with other
251 in-situ instruments (**Tables 2 and 3**). The trailer was situated on the main deck forward of the
252 ship's exhaust stack to avoid contamination. Air was sampled via a VACUUBRAND ME1
253 Diaphragm Vacuum Pump and introduced into the instruments with a ~5 m sampling line. Air for
254 the trailer instruments was drawn from a common inlet ~ 5 m above the ship's bow deck, i.e.,
255 approximately 10 m above the water surface. All continuous in-situ measurements (except VOCs)
256 were recorded at 1-minute intervals.

257 The only instrument requiring calibration during the cruise was the T500U CAPS NO₂ monitor
258 which gave consistently high-quality data. It was first calibrated on the ship on 9 May before
259 sailing from LUMCON. The instrument was fed zero air and measured +0.072 ppbv. The
260 instrument was calibrated to zero. One hundred ppbv NO₂ using the Serinus Cal 2000 gas
261 calibrator and an EPA Protocol gas calibration cylinder was then fed into the instrument, and it
262 read 98 ppbv (calibrated to 100 ppbv). After the cruise, this same single-point calibration was
263 performed again on the ship on 18 May. The zero read -0.06 ppbv, and the 100 ppbv level read

264 100.5 ppbv. A correction to the zero level was applied to account for a small drift from 0.00 to -
265 0.06 ppbv over the cruise period. A correction to the 100 ppbv level was therefore not necessary.

266 The Pandora instrument is a ground-based UV-VIS spectroscopic instrument that provides high
267 spectral and temporal resolution measurements of various trace gases (*Herman et al.*, 2009). In
268 order to retrieve columnar trace gas amounts, spectra are analyzed using the Differential Optical
269 Absorption Spectroscopy technique (DOAS; *Platt and Stutz*, 2008). Spectral measurements can be
270 made using direct-sun/lunar (DOAS) and sky scan (Multi-Axis DOAS, MAX-DOAS)
271 measurement modes to retrieve trace gases columns and profiles, respectively. Direct sun
272 measurements were made during SCOAPE to ensure high temporal resolution and lower AMF
273 uncertainties, allowing for more rigorous comparisons with space-based remote sensing
274 measurements. The integration time was variable during each day based on the measurement
275 schedule design. During the beginning and end of the day, the integration time ranged between 2
276 and 5 milliseconds. During the majority of daylight hours, the integration time ranged between 10
277 and 15 milliseconds.

278 Standard Pandora data products, total column O₃ and NO₂, were all processed using BlickP
279 v1.7.16. Total column NO₂ measurements, which are used in this work, have an accuracy of 0.05
280 DU (2.7×10^{15} molec-cm⁻²; *Luftblick*, 2021). All data were filtered using the L2 data quality flags
281 (DQF) to include only data with high (0 or 10) or medium quality (1 or 11) (*Luftblick*, 2019a,b).
282 Pandora TC NO₂ observations were resampled to 5-min averages for comparison to other
283 measurements.

284 The three NASA Pandora instruments deployed for SCOAPE featured the latest hardware and
285 software upgrades available at that time (*Luftblick*, 2021). Each of these Pandoras (designated as
286 P66, P67, & P68) were assembled at the same time with the most up-to-date instrument computer
287 (Cincoze DC-1100), internal electronics (e.g. relay board, microcontroller), and tracker (LuftBlick
288 TR1). Compared to the original tracker, the new Pandora tracker responds faster, has smoother
289 movements, higher range of motion, and updated software for monitoring of the absolute position
290 (*Luftblick*, 2019a,b). The advanced tracker also allows integration of a head sensor camera,
291 enabling accurate sun tracking on a moving platform, a feature that was crucial to making high-
292 quality column measurements onboard the *R/V Point Sur*. These data could be directly compared
293 to satellite measurements.

294 In addition to the three Pandoras having similar hardware and software, the calibration
295 approach was standardized for the instruments. Field calibration, which is necessary for accurate
296 retrievals of total column NO₂, requires obtaining reference spectra from actual field
297 measurements for each Pandora instrument. While the three Pandoras were collocated at
298 LUMCON (Cocodrie, LA) for 4 weeks prior to P66 being deployed to the *R/V Point Sur*,
299 reference spectra for performing the Minimum Langley Extrapolation (MLE) were selected for
300 each instrument using data collected between 17:55:00 UTC and 18:05:00 UTC on 20 April 2019
301 when all three instruments sampled clear skies and low tropospheric NO₂ amounts. A larger range
302 of data (19 days) was then selected, including the date of our reference spectra, as we assume there
303 is a subset of data in the data series that is independent of AMF. The slope of the red lines on the
304 MLE (**Figure S1**) indicates the minimum vertical column at that location, which should be
305 approximately the stratospheric column. This intercept is equal to our slant column reference
306 amount, which can be added to all the slant column data to produce absolute slant columns and
307 eventually divided by the AMF to produce vertical column amounts. There can be variability in
308 the exact slant column reference amount between instruments; however, overall there was good
309 consistency in the slant column reference amounts among the three instruments (**Figure S2**; data
310 taken from *NASA/LARC/SD/ASDC* [2022c]). This rigorous field calibration ensured consistency

311 among instruments and led to very good agreement as shown in **Figure S2**. Time-matched data
312 from P66, P67, and P68 show the reproducibility of the three Pandora instruments during the 4-
313 week LUMCON test period, as illustrated by referencing Pandoras 66 and 68 to Pandora 67.
314 Agreement in terms of slope and offset of the best-fit lines, as shown in the lower right box in
315 **Figure S2**, is excellent. The correlation coefficient, R , is lower for Pandora 66 because, as the blue
316 symbols show, the latter instrument is slightly noisier than the other two. **Figure S3** displays
317 comparisons of the three Pandora instruments inclusive of the pre-cruise period along with
318 Pandoras 67 and 68 that remained at LUMCON during the cruise period. Overpass comparisons
319 for TROPOMI (gold diamonds) and OMI (magenta triangles) are also shown. Mean Pandora-
320 TROPOMI TC NO₂ offsets are ~13% (**Figure S3**), with the Pandora measuring higher column
321 amounts than TROPOMI. There is more scatter among the three Pandoras during a cloudy period
322 before the cruise on 4 through 8 May 2019 (**Figure S2**).

323 2.2. Other Surface-based Observations

324 Routine meteorological parameters (temperature, relative humidity, winds), which were
325 provided by the *Point Sur*, and continuous NO₂, O₃, CH₄, and CO₂ data were collected during
326 SCOAPE (**Table 2**). We averaged all in-situ NO₂ observations to 5-minutes to match the 5-minute
327 Pandora averages. Uncertainties for these instruments specified in *Martins et al.* (2016) and
328 *Kollonige et al.* (2018) are 5% for NO₂ and 1.3% for O₃. Surface NO₂ and Pandora TC NO₂ spikes
329 that were obviously caused by sampling of the *Point Sur* exhaust were removed from analyzed
330 data as follows. Plume_flag_1 in the SCOAPE data archive marks times when relative winds were
331 from 135 to 225 degrees (blowing from exhaust stack to front of ship) and relative wind speeds
332 were less than 5 m/s. Plume_flag_2 was chosen to eliminate coincident spikes in O₃ (downward)
333 and NO₂ (upward). Analyses of authentic NO₂ spikes are presented in **Section 3.3**.

334 Whole-air, evacuated stainless steel canisters for a large suite of VOC species, CH₄, and CO
335 measurements were filled 2–3 times each day on the *Point Sur* for post-cruise analyses. They were
336 analyzed by the Rowland-Blake research group (*Colman et al.*, 2001) for a range of alkanes,
337 alkenes, aromatics, halogenated carbon species, CO, CH₄, dimethylsulfide and other trace gases.
338 Because of the real-time CO analyzer failure, we report CO data from the flasks only. Subsamples
339 of each canister were transferred via vacuum line to 12 mL evacuated glass vials for stable isotope
340 analysis ($\delta^{13}\text{C}$ and δD) via isotope ratio mass spectrometry (IRMS) at the University of Cincinnati
341 via the method of *Yarnes* (2013). The IRMS instrument is calibrated several times daily with
342 standards bracketing the isotopic composition of samples and with standards matched to the
343 concentration of samples to avoid linearity issues. The reproducibility of $\delta^{13}\text{C}$ and δD is 0.2‰ and
344 4‰, respectively.

345 Flask sampling on the *R/V Point Sur* was normally coordinated with a platform encounter. For
346 large platforms, when a plume downwind was intercepted, as denoted by simultaneous NO₂ and
347 CO₂ spikes, a flask was exposed to collect an air sample. The platform was circled and the process
348 repeated to get an upwind sample. For smaller operations closer to shore (10-11 May and 16-17
349 May in **Figure 1**), plumes were more frequent and maneuvers for contrast sampling were not
350 practical. When the *R/V Point Sur* was near shore a number of flask collections were coordinated
351 with flask fillings on land, 11-17 May, e.g. at Venice, Port Fourchon and other sites shown by red
352 pins in **Figure 1**. Several flasks were filled during a circling of the LOOP on 17/18 May.

353 Boundary-layer information was supplied by Intermet-1-RSB radiosondes launched once or
354 twice daily from 11-17 May. In most cases En-Sci electrochemical concentration cell ozonesondes
355 were launched with the radiosondes; the ozonesonde sensing solution was the 0.5% KI, half-buffer
356 variant (*Thompson et al.*, 2019b). The nominal launch time was midday, near the OMI and
357 TROPOMI overpass time. On four days of the cruise, 14 May, 15 May, 16 May and 17 May,

358 ozonesondes were also launched earlier in the day when the boundary-layer height was near its
359 daily minimum as indicated by the shipboard ceilometer (**Tables 2 and 3**).

360

361 **2.3 Meteorological Forecasts, Reanalysis and Trajectories**

362 To monitor the meteorological conditions throughout the cruise, the Global Modeling and
363 Assimilation Office (GMAO) provided near-real-time support
364 (https://gmao.gsfc.nasa.gov/field_campaigns/past_campaigns) with weather forecasts and data
365 assimilation products from Global Earth Observing System (GEOS) – Forward Processing
366 (GEOS-FP; <https://fluid.nccs.nasa.gov/weather/>) and composition forecasts with their GEOS –
367 Composition Forecasts (GEOS-CF) products (<https://fluid.nccs.nasa.gov/cf/>). Both the FP and CF
368 products were used in making fine adjustments to the cruise track as they indicated two different
369 meteorological regimes while the *Point Sur* was sampling.

370 Post-analysis used the Modern-Era Retrospective analysis for Research and Applications
371 Version 2 (MERRA-2) reanalysis, which is driven by the GEOS-5 atmospheric data assimilation
372 system with $1/2^\circ \times 2/3^\circ$ resolution and 72 layers, to demonstrate the large-scale changes in
373 meteorological conditions during the SCOAPE cruise and the impact on the *R/V Point Sur* in
374 transit (**Section 3.1**). To trace source regions for air arriving at the *R/V Point Sur*, we initialized
375 12-hour ensemble back trajectories using the Hybrid Single-Particle Lagrangian Integrated
376 Trajectory model (HYSPLIT; <https://www.arl.noaa.gov/hysplit/>) developed by NOAA’s Air
377 Resources Laboratory (*Stein et al.*, 2015), driven by National Centers of Environmental Prediction
378 (NCEP) Global Data Assimilation System (GDAS) meteorology every 3 hours at 0.5° resolution
379 at 50 m and 500 m above sea level (**Section 3.2.3**).

380

381 **3. Results and Discussion**

382

383 **3.1 Meteorological Overview of Two Regimes: Marine and Continental Air Masses**

384 The GOM study region during the cruise period of 10-18 May 2019 was characterized by two
385 distinct meteorological regimes. These consisted of primarily onshore (10 to 13/14 May;
386 “marine”) and offshore (14-18 May; “continental”) flow that led to contrasts in the chemical
387 composition. The change in large-scale conditions originated from a weak frontal system that
388 drifted northwest to southeast through the GOM during the middle of the cruise. The progression
389 of the frontal system is presented in **Figure 2**, with MERRA-2 reanalysis mean sea-level pressure
390 (MSLP; black contours), 1000 hPa wind vectors (arrows) and specific humidity (q ; colors) shown
391 for 12 UTC (06 LST; the *Point Sur* position is the red dot). The entire 10-18 May SCOAPE track
392 is overlaid in cyan.

393 The onshore flow “marine” period dominated the first few days of the cruise with easterly to
394 southerly winds and high humidity. The 12 and 13 May snapshots in **Figures 2a** and **2b** display
395 the contrast in wind direction and speed, and humidity along the frontal boundary. The event was
396 analyzed as a cold front by NOAA’s Weather Prediction Center
397 (https://www.wpc.ncep.noaa.gov/archives/web_pages/sfc/sfc_archive_maps.php?arcdate=05/13/2019&selmap=2019051312&maptpe=namussfc). Specific humidity values increased by nearly a
399 factor of two from northwest ($\sim 10 \text{ g kg}^{-1}$) to southeast ($\sim 20 \text{ g kg}^{-1}$), with a corresponding change
400 in the wind direction/source region across the front. On 13 May, the *Point Sur* (red dot on **Figure**
401 **2b**) sat in a transition zone along the front and in between the two distinct air masses. After 13
402 May, the frontal boundary pushed farther southeast into the GOM, and the wind direction became
403 northeasterly/easterly (**Figures 2c,d**), with trace gas measurements from the ship and satellite data
404 indicating sources from more polluted, “continental” regions. Detailed analysis of the effects of

405 the two large-scale meteorological regimes on the cruise pollution measurements follow in
406 **Sections 3.2 and 3.3.**

407 408 **3.2 Chemical Composition in Two Regimes: Unpolluted Marine and Moderately Polluted** 409 **Continental**

410 3.2.1 Satellite Views of Total Column (TC NO₂)

411 Satellite column data (TC NO₂ in **Figure 3**) capture the contrast of the two regimes. Cloud
412 cover precluded extensive retrievals over much of the open GOM on 13 and 15 May for OMI
413 (**Figures 3a and 3b**). Both OMI and TROPOMI measurements for 13 May displayed relatively
414 low levels of TC NO₂ except for values of TC NO₂ > 0.20 DU over the New Orleans and Baton
415 Rouge areas (red and orange in **Figures 3c and 3e**). For 15 May, after the wind shift brought
416 continental air offshore (**Figures 2c and d**) and cloud cover retreated (mostly < 0.1, **Figure 3b**),
417 the urban regions and the adjacent GOM registered widespread pixels with readings exceeding
418 0.15 DU TC NO₂ (**Figures 3d and f**). The satellite maps in **Figure 3** display overall OMI and
419 TROPOMI similarities but detailed comparison of TC NO₂ also highlights some differences, the
420 horizontal resolution of the two sensors being the most obvious. Individual orange-to-red pixels
421 recorded by TROPOMI on 15 May (**Figure 3f**) may indicate NO_x sources over land and the
422 adjacent GOM where small platforms are concentrated (**Figure 1**). However, TROPOMI retrievals
423 run ~ (0.03-0.05) DU greater than the corresponding TC NO₂ OMI readings, primarily along the
424 coast but also over GOM between 27.0°N and 28.5°N latitude. These differences are evaluated
425 with the shipboard Pandora 66 (P66) and the two Pandoras (P67, P68) at LUMCON (**Section**
426 **3.3.3**).

427 Not all NO₂ pollution observed by satellites and on the *R/V Point Sur* during the transition of air
428 masses on 13-14 May was from the nearby region. Starting on 13 May, the cruise encountered air
429 originating from Mexican agricultural fires upwind of the ship. **Figure S4** shows elevated
430 MODerate resolution Imaging Spectrometer (MODIS) aerosol optical depth (AOD; *Naval*
431 *Research Laboratory and the University of North Dakota/MODIS Adaptive Processing System*
432 (*MODAPS*), 2017) as dark reds in false color transported northward into the SCOAPE cruise
433 region from areas of concentrated fire counts derived from MODIS and Suomi National Polar-
434 Orbiting Partnership (Suomi NPP) Visible Infrared Imaging Radiometer Suite (VIIRS; *Giglio and*
435 *Justice*, 2021; *Schroeder and Giglio*, 2017) observations (orange and red dots in Mexico). The
436 Atmospheric Infrared Sounder (AIRS; *AIRS Science Team/Joao Teixeira*, 2013) captured elevated
437 mid-tropospheric CO plumes from Mexico in the vicinity of the SCOAPE cruise on 13-14 May
438 (**Figure S5**). Precise NO₂ source attribution is beyond the scope of this study, but we note that the
439 GEOS-CF model forecast used during the cruise identified a CO-fire tracer originating from
440 Mexico over the SCOAPE sampling region on 14 May (not shown).

441 3.2.2 Shipboard Measurements of Ozone and Other Trace Gases

442 The switch from clean marine air to a more continental influence is reflected in a number of
443 constituents. **Figure 4a** shows that late on 13 May there was an abrupt transition in wind direction
444 (gray line) measured on the ship from mostly south/southwest to north/northeast. Surface ozone
445 (blue line) increased from 20 ppbv or less to more than 40 ppbv, with peak readings of >70 ppbv
446 on 16–17 May (note back-trajectories from ship location on 15 and 17 May, **Figure S6**). The
447 lowest ozone values measured at the beginning of the cruise, 10-13 May 2019, are referred to as
448 having air of “marine” origins (**Figure 2**). After 13 May the air is designated as “continental” with
449 the high-ozone levels on the last days occurring in the westernmost segment of the track (**Figure**
450 **1**). Surface CO from shipboard canister samples (**Figure 4b**) also reflects the marine vs
451 continental classification. Prior to 13 May, CO mixing ratios from 7 measurements range from 55-

452 95 ppbv, levels associated with the equatorial Atlantic (*Thompson et al.*, 2000). After 13 May the
453 canister samples range from 100 ppbv to 170 ppbv CO, with a mean value of ~130 ppbv for the
454 period 14-18 May. Daily CO mixing ratios from the canister samples (**Figure 4b**) abruptly
455 changed from “marine” values of ~80 ppbv to ~120 ppbv on 13 May, when the *Point Sur*
456 encountered air parcels from the Mexican fires. Mixing ratios of CO remain elevated on 14 May
457 when an aerosol plume from the fires was transported to the *Point Sur* (**Figure S4b**). AIRS CO
458 (**Figure S5**) shows a similar movement of fire pollution from 13 to 14 May although much of the
459 ship sampling area is obscured by clouds. **Figure 4b** displays shipboard surface NO₂. The overall
460 marine vs continental contrast is present but there are many pollution spikes in the “marine”
461 period of the cruise when the *Point Sur* was sampling near platforms, usually within 1.5-2 km (1
462 and 2 labels in **Figure 4b**; **Figure 1**). Elevated NO₂ measurements from the ship analyzer were
463 found between Brutus and Atlantis and southwest of the Mars/Olympus platforms (labels 3-5 in
464 **Figure 4b**; **Figure 1**).

465 The ozonesonde ozone mixing ratio curtain (**Figure 5**) captures the complex vertical structure
466 of air passing over the *Point Sur*. During the “clean marine” phase the sharp ozone gradient seen at
467 15 km on 12–14 May is typical of the tropopause in tropical air. The low-ozone layer between 10
468 and 14 km may originate from convective redistribution of air from the surface to cloud-outflow
469 level (*Petropavlovskikh et al.*, 2010; *Thompson et al.*, 2010; *Thompson et al.*, 2012). The
470 continental air, in contrast, that displays a tropopause closer to 10 km and ozone greater than 80
471 ppbv, is pervasive above 3 km. In addition, the mid-troposphere includes ozone of stratospheric
472 origins (note shift to very low water vapor, **Figure S7**), which is common in spring.

473 A snapshot of marine vs continental influences for CH₄, CO, CO₂ and dimethylsulfide (DMS)
474 concentrations, based on the 27 *Point Sur* flask samples, appears in **Figure 6**. DMS is of marine
475 biogenic origin, so it is greater in the first part of the cruise, up to 14 May, than in the latter part.
476 Species with continental biogenic origin (isoprene, α - and β -pinene, not shown) exhibit the
477 opposite pattern. **Figure 7** summarizes the relationship between ethane and CH₄ as well as $\delta^{13}\text{C}$
478 and δD for both regimes based on 15 flask samples offshore and 2 flask samples onshore. Both
479 CH₄ isotopes (**Figure 7a**) show small changes to more negative values during the shift from
480 marine to more continental air (**Figure 7b** displays sample locations). Ratios in **Figure 7** represent
481 enhancements above mean CH₄ and ethane campaign values. The highest enhancement ratios are
482 observed after 14 May in the vicinity of the far eastern shallow and deep-water platforms (e.g.,
483 Petronius, Point 6 in **Figures 4b** and **7b**, with moderate CO and relatively low surface NO₂) and
484 the far western shallow-water platforms (**Figure 7b**). This distribution is similar to previous
485 limited GOM sampling, e.g., *Yacovitch et al.* (2020). Note that the two onshore samples show
486 more negative $\delta^{13}\text{C}$ and δD compared to all the samples from the *Point Sur*.

487 An extreme example of air polluted with high VOC was captured in a canister sample collected
488 near a shallow-water platform at 1612 Local Time (LT) Central Daylight Time (CDT) on 16 May.
489 **Figure 7a** shows that an elevated C₂H₆/CH₄ occurred with the most ¹³C-depleted sample. **Figure**
490 **7b** depicts the location of that sample in the far western region of shallow water platforms (Point 7
491 in **Figure 4b**). **Table 4** gives concentrations of representative carbon-containing compounds in the
492 16 May flask. The CH₄ increase was a factor of ~3 greater than the median of 27 flasks collected
493 during the entire cruise. This concentration signified leaks from gas production; the CO₂ from the
494 same flask was nearly identical to the all-cruise CO₂ flask median. However, ethane, n-propane
495 and benzene amounts were 75, 130, and 45 times higher, respectively, than their cruise averages.

496 3.2.3 Trajectory Analysis

497 Although the examples in **Figures 4-7** illustrate considerable hour-to-hour variability in all the
498 constituents measured, a contrast in overall air quality before and after 14 May 2019 dominates the

499 chemical character of the GOM during SCOAPE. This is supported by air parcel trajectory
500 analysis carried out with HYSPLIT driven by NCEP GDAS at 0.5° resolution. The trajectories
501 were initialized at the start time of VOC canister sampling to help with source attribution. **Figure**
502 **8** displays ensemble 12-hour back trajectories initialized at the indicated LT (CDT) 50 m above
503 sea level (upper panels) and 500 m (lower panels) with red, green, and blue air parcels denoting a
504 change in release time of every 3 hours over the 12-hour period. The marine regime observed by
505 the *Point Sur* coincides with onshore flow, indicated by winds from the south-southeast on 10-12
506 May as shown in **Figures 8a** and **8d** (12 May 2019 back trajectories at 0900 LT CDT) and **Figure**
507 **4a** in situ data. The continental regime observed after the start of 14 May indicates the wind shift
508 from the north-northeast (**Figure 4a** in situ data). The corresponding trajectories appear in **Figures**
509 **8c** and **8f** on 14 May at 1700 LT CDT. May 13 marked a transition period between these two
510 regimes (**Figure 2b**). The change in wind direction viewed in **Figures 8b** and **8e** captures the
511 Mexican fire influence (southwest origins; cf **Figures S4** and **S5**) detected on the *Point Sur* prior
512 to the 14 May shift to north-northeasterly winds on 14 May. **Figure S6** provides insight into
513 changing winds during the continental regime, 15-17 May. During that period, back trajectories
514 show air originating from along shore sources (e.g., shallow-water platforms, LOOP), as in the
515 extreme pollution measured in the 16 May canister (**Figure 7** and **Table 4**).

516

517 3.3 Satellite, Pandora and Surface NO₂ During Two Regimes on SCOAPE

518 **Figures 9** and **10** illustrate TC NO₂ variability during the SCOAPE cruise, with observations
519 from P66, TROPOMI and OMI. **Figure 9**, that illustrates all the 5-min average P66 readings,
520 presents a comparison of the 7 full days of SCOAPE (11-17 May). TROPOMI overpass TC NO₂
521 values (diamonds for color-coded days) are also shown. Transient spikes in P66 TC NO₂ are more
522 prevalent after the wind shift on 13 May (note the transition to higher TC NO₂ values on 14 May
523 in the green circles after 1800 local time, **Figure 9**). These signify an encounter with a local NO₂
524 source, presumably corresponding to label 5 where the *Point Sur* had its second encounter with the
525 Mars/Olympus complex. At the same time, label 5 in **Figure 4b** shows that flask CO rose to 130
526 ppbv and the surface NO₂ analyzer measured more than 20 ppbv. Most of the P66 TC NO₂
527 observations on 11-13 May (red-orange, gold, purple circles in **Figure 9**) are below 0.18 DU and
528 no individual data point exceeds 0.20 DU. Where label 1 appears (gold circles, at the first pass of
529 Mars/Olympus complex) surface NO₂ spikes to > 10 ppbv but CO is only moderately elevated
530 (100 ppbv in **Figure 4b**). After the shift to offshore winds, in contrast, from 15-17 May, except for
531 ~0700, all P66 TC NO₂ readings are above 0.18 DU with most transient spikes displaying TC NO₂
532 > 0.22 DU. There is no consistent diurnal variation across the days although the proportion of
533 spikes is greater early in the day on 15-17 May (dark red and blue circles in **Figure 9**) when the
534 ship was near shore near a high density of platforms. An exception was near Petronius (label 6 in
535 **Figure 9**). Tracers of pollution do not always correlate. **Figure 4b** (Label 6) shows moderately
536 elevated CO near the large Petronius platform and greatly enhanced ethane/CH₄ (easternmost
537 point in **Figure 7b**). However, Label 6 in **Figure 4b** shows that surface NO₂ was < 5 ppbv.
538 Petronius is not far from shore and a high density of smaller platforms. The Pandora may be
539 responding to pollution layers aloft from the latter source; that would also be consistent with
540 elevated VOC from leakage.

541 There were five TROPOMI overpass columns (diamonds in **Figure 9**) during the cruise, two on
542 11 and 13 May 2019 (orange-red and purple diamonds), that agreed within 0.03 DU of the
543 coincident P66 TC NO₂ values. The triangles in **Figure 9** signify OMI readings for 11, 12 and 13
544 May 2019. The 11 and 13 May OMI TC NO₂ values (orange-red and purple triangles) are 0.02-
545 0.03 DU lower than their TROPOMI counterparts; this is very good agreement considering the

546 different resolution of the two satellite instruments. On 12 May, near the overpass time, 1450
547 local, both P66 and OMI (gold triangle) measured 0.16-0.18 DU; there was not a TROPOMI
548 observation that day. The three TROPOMI readings on 15-17 May give TC NO₂ ~0.16 DU
549 compared to P66 TC NO₂ values ~0.20 DU. The OMI TC NO₂ readings for 15 and 17 May are
550 0.17 DU, virtually the same as for TROPOMI. For both OMI and TROPOMI during the 15-17
551 May period, the satellite TC NO₂ measurements are ~20% lower than those of the Pandora.

552 **Figure 10a** compares P66 and satellite TC NO₂ with in-situ NO₂ observations during the
553 cruise. The overall underestimate of OMI and TROPOMI satellite columns relative to P66 on 15-
554 17 May (cf. **Figure 9**) is striking. The in-situ NO₂ values roughly follow the two-regime pattern,
555 with surface NO₂ increasing ~50% after 14 May. However, most individual surface NO₂ spikes
556 during plume encounters are not detected simultaneously by the Pandora. **Figure 10a** shows that
557 P66 may observe elevated TC NO₂ in advance of an in-situ NO₂ spike on the *Point Sur* (e.g., labels
558 1, 4 and 7) but Label 5 is the opposite. For Label 6 (near Petronius, **Figure 4b** and **9**), the high P66
559 measurements are not reflected in the shipboard NO₂ readings. Decoupling between ambient and
560 column NO₂ can occur when the boundary layer is not well-mixed, i.e., high NO₂ trapped near the
561 surface may not be observed in the Pandora column. Mismatches can also result when much of the
562 NO₂ column is an above-mixed layer residual or is advected from upwind (*Thompson et al.*,
563 2019a). **Figure 10a** illustrates the complexity of surface-TC NO₂ relationships. For example, 15
564 May is the day with the greatest range in TC NO₂ values (cf. **Figure 9**, Label 6 and paler blue
565 circles throughout the day). There is a slow increase in P66 TC NO₂ during the morning hours
566 (before the overpass symbols) with a few ship NO₂ spikes less than 5 ppbv (**Figure 10a**). The P66
567 TC NO₂ readings are in a range (0.17 ±0.02) DU except for 4 green dots, three of them ~0.30 DU.
568 In the afternoon of 15 May there are a number of in-situ NO₂ ship spikes > 20 ppbv, i.e. more than
569 a 4-fold increase from the morning values. A shipboard canister sample from 15 May, ~1500 LT
570 while passing the Petronius platform, indicated n-butane and i-pentane (species associated with
571 flaring) that were the second highest of the campaign. However, the corresponding P66 afternoon
572 values are confined to a 0.17-0.28 DU range, only a ~50% variation and at most a factor of 2
573 increase from the morning. On 16 May while passing shallow water platforms (cf **Figure 1**), the
574 afternoon *Point Sur* shipboard spikes (Label 7 in **Figure 10a**) are higher than on 15 May (near
575 northeastern platforms, cf **Figure 1**) but the corresponding P66 TC NO₂ measurements do not
576 exceed 0.20 DU.

577 The NO₂ column densities and locations of P66 along the ship track are illustrated in **Figure**
578 **10b**. The location of the pre-15 May segments, mostly below 0.16 DU (green and blue dots), was
579 in the deepwater platform area sampled with onshore winds (**Figures 2** and **8a,d,e**). After 15 May,
580 when P66 registered numerous segments with TC NO₂ > 0.18 DU, sampling was closer to shore in
581 the vicinity of platforms like Petronius and a high-density of small natural gas operations in the
582 northeastern and westernmost regions (orange to red in **Figure 10b**).

583 A summary of overpass comparisons from OMI and TROPOMI TC NO₂ relative to the
584 shipboard Pandora 66 appears in **Figure 11**. Although the TROPOMI satellite instrument footprint
585 is smaller than that of the OMI satellite, the offsets with P66 are nearly the same. During
586 SCOAPE, a significant factor affecting Pandora-satellite agreement, summarized in Tables S1 and
587 S2, was clouds. TROPOMI during 11-13 May, the cloudiest period of the cruise, recorded 20%
588 higher TC NO₂ than the LUMCON P67 and P68 (tan-orange shaded diamonds in **Figure 11**),
589 likely due to increased uncertainty in cloud correction in NO₂ retrievals. Otherwise, the satellite
590 and Pandora TC NO₂ comparisons for clear-sky conditions agreed within 5%. A second factor
591 influencing agreement was the satellite retrieval over water. As the P66 TC NO₂ measurements
592 increased during 15-17 May (all symbols with Pandora TC NO₂ > 0.19 DU in **Figure 11**), the

593 offsets were as large as 25% (satellite data low), even in cloud-free conditions. In **Figure 11**, the
594 satellite data with TC NO₂ ≤ 0.18 DU averaged within 5% of the land and ship Pandoras.4.

595 **Summary and Conclusions**

596 The May 2019 SCOAPE cruise, conducted with the *R/V Point Sur* in a region rich in oil and
597 natural gas activity off the Louisiana coast, has been described. Designed to determine the
598 feasibility of using satellite data to measure AQ with TC NO₂ as the key pollutant, SCOAPE
599 addressed both scientific and technological questions.

600 • *What do pollutant levels measured by satellite over the GOM look like, and how do they*
601 *compare to coastal Louisiana? What role does meteorology play in any observed differences?*

602 During our May 2019 sampling, on a regional basis, the OMI and TROPOMI satellites showed
603 that TC NO₂ was greater over the continent and near-coastal areas than deepwater segments of the
604 cruise. This picture of two AQ regimes, one from 10-13 May and the second from 14-18 May, was
605 consistent with tracers measured on the ship (ozone, CO, VOC) and contrasting meteorology
606 during the two periods.

607 • *Can satellite observations detect emissions from ONG operations, and are the measurements*
608 *accurate?* The OMI and TROPOMI satellites detected elevated NO₂ from ONG operations on a
609 regional basis but emissions from individual platforms could not be characterized. This limitation
610 was due to a combination of satellite spatial resolution, once-daily overpasses, moderately high
611 cloud cover and low to moderate pollution levels over the GOM. Referenced to both land- and
612 ship-based Pandoras, satellite TC NO₂ *on average* was accurate to ~5% and ~13%, respectively,
613 with the satellite biased low at the higher pollution levels (differences ~20%). Under clear-sky
614 conditions agreement between satellites and the Pandoras was 2-3% over the coastal site.

615 • *How accurately do Pandora NO₂ readings track short-term variations in ONG emissions?*

616 *What is the precision of the new-model Pandora instruments that were deployed during SCOAPE?*

617 Through most of a day's sampling, P66 TC NO₂ responds to mixed-layer NO₂ variability as
618 measured with the ship's analyzer. However, timing and magnitude of the Pandora and in-situ
619 NO₂ responses are typically offset due to the viewing characteristics of the spectrometer. The
620 magnitude of one set of P66 TC NO₂ enhancement was ~50% when corresponding NO₂ plumes
621 registered a 4-fold increase at the surface. In the first evaluation of Pandora TC NO₂ precision,
622 three Pandora instruments, Nos. 66, 67, and 68, operating at Cocodrie, LA, for 4 weeks prior to
623 the cruise, were found to agree within 5% (~0.01 DU) of one another.

624 • *Is there a difference in pollutant emissions between large, deepwater ONG platforms and*
625 *the hundreds of small near-shore ONG operations?* There were strong responses in surface and
626 Pandora NO₂ to both deepwater and near-shore operations. The canister sampling confirmed that
627 near-shore platforms leak methane and other VOC associated with natural gas extraction and the
628 deepwater platforms do not because they flare the gas.

629
630 Our analysis of the SCOAPE data has not been exhaustive, leaving room for future work. For
631 example, the LUMCON Pandora data have not been compared to surface NO₂ data or the VOC
632 samples. Evaluating the degree to which Pandora TC NO₂ amounts correlate with surface NO₂ in
633 the GOM is a topic for further investigation. Matching the variability to sources will require
634 analysis with in-situ tracers, ancillary satellite data, air parcel trajectories and, where possible,
635 model output. Better statistics for the column-surface NO₂ connection and characterization of the
636 environmental conditions for which the link is strongest will prepare us for optimal usage of NO₂
637 and ozone data from the upcoming geostationary Tropospheric Emissions: Monitoring of Pollution
638 (TEMPO) satellite instrument that is designed for hourly pollution monitoring over North
639 American coastal waters.

640
641
642
643
644
645
646
647
648
649
650
651
652
653
654
655
656
657
658
659
660
661
662
663
664
665
666
667
668
669
670
671
672
673
674
675
676
677
678
679
680
681
682
683
684
685
686
687
688
689
690
691
692
693
694
695
696

Acknowledgments

We are very grateful to Capt. Nick Allen, First Mate J. D. Ellington and the entire crew of the *R/V Point Sur* and extraordinary support and hospitality from LUMCON as well as to N. Dačić (SSAI @ NASA) and V. J. Maisonet-Montañez (BOEM) for on-board measurement assistance. We thank the NASA Earth Sciences Division Tropospheric Composition Program (B. Lefer) for its support of the NASA Pandora Project as well as ESA/NASA's Pandonia Global Network and Luftblick for processing the Pandora data. This study was partially funded by the U.S. Department of the Interior, Bureau of Ocean Energy Management through Interagency Agreement M17PG00026 with NASA (B. Duncan, PI). Additional support came from the NASA HQ Applied Sciences Program (J. Haynes).

Data Availability Statement

The satellite data were downloaded as follows: OMI total NO₂ column data from the NASA GES DISC at https://aura.gesdisc.eosdis.nasa.gov/data/Aura_OMI_Level2/OMNO2.003 (<https://doi.org/10.5067/Aura/OMI/DATA2017>; Krotkov et al., 2019), TROPOMI total NO₂ column data from <https://scihub.copernicus.eu/> (<https://doi.org/10.5270/S5P-s4ljg54>; Copernicus Sentinel-5P, 2018), and <https://worldview.earthdata.nasa.gov> provided the AIRS (AIRS Science Team/Joao Teixeira, 2013), SNPP VIIRS (Schroeder and Giglio, 2017), and MODIS products (Giglio and Justice, 2021; Naval Research Laboratory and the University of North Dakota/MODIS Adaptive Processing System (MODAPS), 2017). The SCOAPE data used here are available through the NASA/Langley Research Center Atmospheric Data Center as follows: the surface data from the LUMCON observations were retrieved from NASA/LARC/SD/ASDC (2022a); https://doi.org/10.5067/ASDC/SUBORBITAL/SCOAPE_Ground_Data_1), the ship data from NASA/LARC/SD/ASDC (2022b); https://doi.org/10.5067/ASDC/SUBORBITAL/SCOAPE_RVPointSur_Data_1) and the Pandora data from NASA/LARC/SD/ASDC (2022c); https://doi.org/10.5067/ASDC/SUBORBITAL/SCOAPE_Pandora_Data_1). The ozonesonde profile data are downloadable from NASA/LARC/SD/ASDC (2022d); https://doi.org/10.5067/ASDC/SUBORBITAL/SCOAPE_Sondes_Data_1). Hysplit back trajectories (Stein et al., 2015) were run online via here: <https://www.ready.noaa.gov/hypub-bin/trajtype.pl?runtype=archive>. All analyses were performed using the MATLAB 2022a/b software packages (<https://www.mathworks.com/help/matlab/release-notes.html>; MATLAB, 2022).

References

- Adelman, Z. E., Pierce, R. B., Stanier, C. O., and Kenski, D. M.: LMOS: 2017 Lake Michigan Ozone Study, EM: Air and Waste Management Association's Magazine for Environmental Managers, ISSN: 2470-4741, Vol. 2020, Issue October, 2020.
- AIRS Science Team/Joao Teixeira (2013). AIRS/Aqua L2 Standard Physical Retrieval (AIRS-only) V006 Carbon Monoxide, NASA Worldview Earthdata, Retrieved from <https://worldview.earthdata.nasa.gov> and <https://doi.org/10.5067/Aqua/AIRS/DATA202>.
- Boersma, K. F., Eskes, H. J., Veeffkind, J. P., Brinksma, E. J., van der A, R. J., Sneep, M., van den Oord, G., H., J., Levelt, P. F., Stammes, P., Gleason, J. F., and Bucsele, E. J. (2007). Near-real time retrieval of tropospheric NO₂ from OMI. *Atmospheric Chemistry & Physics*, 7, 2103-2118, <https://doi.org/10.5194/acp-7-2103-2007>.
- Boersma, K. F., Eskes, H. J., Dirksen, R. J., van der A, R. J., Veeffkind, J. P., Stammes, P., et al. (2011) An improved tropospheric NO₂ column retrieval algorithm for the Ozone Monitoring Instrument, *Atmospheric Measurement Techniques*, 4, 1905–1928, <https://doi.org/10.5194/amt-4-1905-2011>.
- Boersma, K. F., Eskes, H. J., Richter, A., De Smedt, I., Lorente, A., Beirle, S., et al. (2018) Improving algorithms and uncertainty estimates for satellite NO₂ retrievals: Results from the quality assurance for the essential climate variables (QA4ECV) project, *Atmospheric Measurement Techniques*, 11, 6651–6678, <https://doi.org/10.5194/amt-11-6651-2018>.
- Burrows, J. P., Weber, M., Buchwitz, M., Rozanov, V., Ladstaetter-Weissenmayer, A., Richter, A., DeBeek, R., Hoogen, R., Bramstedt, K., Eichmann, K. U., Eisinger, M., Perner, D. (1999) The global ozone monitoring experiment (GOME): Mission concept and first scientific results, *Journal of Atmospheric Sciences*, 56, 151–175.
- Choi, S., Lamsal, L. N., Follette-Cook, M., Joiner, J., Krotkov, N. A., Swartz, W. H., et al. (2020) Assessment of NO₂ observations during DISCOVER-AQ and KORUS-AQ field campaigns, *Atmospheric Measurement Techniques*, 13, 2523–2546, <https://doi.org/10.5194/amt-13-2523-2020>.
- Colman, J. J., A. L. Swanson, S. Meinardi, B. C. Sive, D. R. Blake and F. S. Rowland (2001). Description of the Analysis of a Wide Range of Volatile Organic Compounds in Whole Air Samples Collected during PEM-Tropics A and B, *Analytical Chemistry*, 73 (N15), 3723-3731.

697 Copernicus Sentinel-5P (processed by ESA; 2018). TROPOMI Level 2 Nitrogen Dioxide total column products, Version
698 01.3, European Space Agency, <https://doi.org/10.5270/S5P-s4ljg54>.

699 Dačić, N., Sullivan, J. T., Knowland, K. E., Wolfe, G. M., Oman, L. D., et al. (2020). Evaluation of NASA's high-
700 resolution global composition simulations: Understanding a pollution event in the Chesapeake Bay during the summer
701 2017 OWLETS campaign. *Atmospheric Environment*, 222, <https://doi.org/10.1016/j.atmosenv.2019.117133>.

702 Duncan B. N. (2020) NASA resources to monitor offshore and coastal air quality. Sterling (VA): U.S. Department of the
703 Interior, Bureau of Ocean Energy Management. OCS Study BOEM 2020-046. 41 p.

704 Duncan, B., Yoshida, Y., De Foy, B., Lamsal, L., Streets, D., Lu, Z., et al. (2013). The observed response of ozone
705 monitoring instrument (OMI) NO₂ columns to NO_x emission controls on power plants in the United States: 2005-
706 2011. *Atmos. Environ.*, 81, 102-111, <https://doi.org/10.1016/j.atmosenv.2013.08.068>.

707 Duncan, B., Lamsal, L., Thompson, A., M., Yoshida, Y., Hurwitz, M., M., Pickering, K., E., et al. (2016). A space-based,
708 high-resolution view of notable changes in urban NO_x pollution around the world (2005-2014). *Journal of Geophysical*
709 *Research*, 121(2), 976-996, <https://doi.org/10.1002/2015JD024121>.

710 Giglio, L., Justice, C. (2021). MODIS/Aqua Thermal Anomalies/Fire 5-Min L2 Swath 1km V061 [Data set]. NASA
711 Worldview Earthdata. Retrieved from <https://worldview.earthdata.nasa.gov> and
712 <https://doi.org/10.5067/MODIS/MYD14.061>.

713 Goldberg, D. L., Anenberg, S. C., Griffin, D., McLinden, C. A., Lu, Z., Streets, D. G. (2020) Disentangling the impact of
714 the COVID-19 lockdowns on urban NO₂ from natural variability, *Geophysical Research Letters*,
715 <https://doi.org/10.1029/2020GL089269>.

716 Goldberg, D. L., Anenberg, S. C., Kerr, G. H., Mohegh, A., Lu, Z., & Streets, D. G. (2021). TROPOMI NO₂ in the United
717 States: A detailed look at the annual averages, weekly cycles, effects of temperature, and correlation with surface NO₂
718 concentrations. *Earth's Future*, 9(4), e2020EF001665. <https://doi.org/10.1029/2020EF001665>

719 Gronoff, G., Robinson, J., Berkoff, T., Swap, R., Farris, B., Schroeder, J., et al. (2019), A method for quantifying near
720 range point source induced O₃ titration events using co-located Lidar and Pandora measurements, *Atmospheric*
721 *Environment*, 204, 43-52, <https://doi.org/10.1016/j.atmosenv.2019.01.052>.

722 Herman, J., Abuhassan, N., Kim, J., Kim, J., Dubey, M., Raponi, M., and Tzortziou, M. (2019) Underestimation of column
723 NO₂ amounts from the OMI satellite compared to diurnally varying ground-based retrievals from multiple PANDORA
724 spectrometer instruments, *Atmos. Meas. Tech.*, 12, 5593–5612, <https://doi.org/10.5194/amt-12-5593-2019>.

725 Herman, J., Cede, A., Spinei, E., Mount, G., Tzortziou, M., and Abuhassan, N. (2009). NO₂ column amounts from ground-
726 based Pandora and MFDOAS spectrometers using the direct-sun DOAS technique: Intercomparisons and application to
727 OMI validation. *J. Geophys. Res.-Atmos.*, 114(D13), <https://doi.org/10.1029/2009JD011848>.

728 Herman, J., Spinei, E., Fried, A., Kim, J., Kim, J., Kim, W., et al. (2018). NO₂ and HCHO measurements in Korea from
729 2012 to 2016 from PSI spectrometer instruments compared with OMI retrievals and with aircraft measurements during
730 the KORUS-AQ campaign. *Atmos. Meas. Tech.*, 1-60, <https://doi.org/10.5194/amt-2018-56>.

731 Heue, K.-P., Wagner, T., Broccardo, S. P., Walter, D., Piketh, S.J., Ross, K. E., et al. (2008). Direct observation of two
732 dimensional trace gas distributions with an airborne Imaging DOAS instrument, *Atmos. Chem. Phys.*, 8, 6707–6717,
733 <https://doi.org/10.5194/acp-8-6707-2008>.

734 Judd, L. M., Al-Saadi, J. A., Janz, S. J., Kowalewski, M. G., Pierce, R. B., Szykman, J. J., et al. (2019) Evaluating the
735 impact of spatial resolution on tropospheric NO₂ column comparisons within urban areas using high-resolution airborne
736 data, *Atmospheric Measurement Technology*, 12, 6091–6111, <https://doi.org/10.5194/amt-12-6091-2019>.

737 Judd, L., et al. (2020), Evaluating Sentinel-5P TROPOMI tropospheric NO₂ column densities with airborne and Pandora
738 spectrometers near New York City and Long Island Sound, *Atmospheric Measurement Techniques*,
739 <https://doi.org/10.5194/amt-2020-151>.

740 Karambelas, A. (2020) LISTOS: Toward a better understanding of New York City's ozone pollution problem, EM
741 Magazine (Air and Waste Management Assn), Oct 2020.

742 Keabian, P. L., Herndon, S. C., Freedman (2005), Detection of nitrogen dioxide by cavity attenuated phase shift
743 spectroscopy, *Anal. Chem.* 77, 2, 724–728, <https://doi.org/10.1021/ac048715y>

744 Knepp, T., et al. (2015). Estimating surface NO₂ and SO₂ mixing ratios from fast-response total column observations and
745 potential application to geostationary missions, *Journal of Atmospheric Chemistry*, 72(3–4), 261–286,
746 <https://doi.org/10.1007/s10874-013-9257-6>.

747 Kollonige, D. E., Thompson, A. M., Josipovic, M., Tzortziou, M., Beukes, J. P., Burger, R., et al. (2018). OMI satellite
748 and ground-based Pandora observations and their application to surface NO₂ estimations at terrestrial and marine sites,
749 *J. Geophys. Res. Atmos.*, 123(2), 1441-459, <https://doi.org/10.1002/2017JD026518>.

750 Kotsakis, A., Sullivan, J.T., Hanisco, T.F., Swap, R.J., Caicedo, V., Berkoff, T.A., et al. (2022). Sensitivity of total column
751 NO₂ at a marine site within the Chesapeake Bay during OWLETS-2, *Atmospheric Environment*, 277,
752 <https://doi.org/10.1016/j.atmosenv.2022.119063>.

753 Kreher, K., Spinei, E., PETERS, A., Apituley, A., Bais, A., Doerner, S., Fayt, C., Friedrich, M., Frumau, A., Hendrick, F.,
754 Hermans, C., Karagiorgidis, D., Querel, R., Van Roozendaal, M., Vonk, J., and Wagner, T. (2020). MAX-DOAS

755 measurements of atmospheric rural and urban NO₂ gradients during the TROLIX'19 campaign, *EGU General Assembly*
756 *2020*, Online, 4–8 May 2020, EGU2020-20796, <https://doi.org/10.5194/egusphere-egu2020-20796>.

757 Krotkov, N. A., Lamsal, L. N., Celarier, E. A., Swartz, W. H., Marchenko, S. V., Bucsela, E. J., Chan, K. L., Wenig, M.,
758 Zara, M. (2017) The version 3 OMI NO₂ standard product, *Atmospheric Measurement Technology*, 10, 3133–3149,
759 <https://doi.org/10.5194/amt-10-3133-2017>.

760 Krotkov, N. A., Lamsal, L. N., Marchenko, S. V., Bucsela, E. J., Swartz, W.H., Joiner, J. and the OMI core team (2019).
761 OMI/Aura Nitrogen Dioxide (NO₂) Total and Tropospheric Column 1-orbit L2 Swath 13x24 km V003, Greenbelt,
762 MD, USA, Goddard Earth Sciences Data and Information Services Center (GES DISC), Accessed: [March 2022],
763 <https://doi.org/10.5067/Aura/OMI/DATA2017>.

764 Lamsal, L. N., Krotkov, N. A., Celarier, E. A., Swartz, W. H., Pickering, K. E., Bucsela, E. J., et al. (2014). Evaluation of
765 OMI operational standard NO₂ column retrievals using in situ and surface-based NO₂ observations. *Atmospheric*
766 *Chemistry and Physics*, 14(21), 11,587–11,609, <https://doi.org/10.5194/acp-14-11587-2014>.

767 Lamsal, L. N., Janz, S., Krotkov, N., Pickering, K. E., Spurr, R. J. D., Kowalewski, M., et al. (2017) High-resolution NO₂
768 observations from the Airborne Compact Atmospheric Mapper: Retrieval and validation, *Journal of Geophysical*
769 *Research*, 122, 1953–1970, <https://doi.org/10.1002/2016JD025483>.

770 Lamsal, L. N., Krotkov, N. A., Vasilkov, A., Marchenko, S., Qin, W., Yang, E.-S., et al. (2021) Ozone Monitoring
771 Instrument (OMI) Aura nitrogen dioxide standard product version 4.0 with improved surface and cloud treatments,
772 *Atmospheric Measurement Techniques*, 14, 455–479, <https://doi.org/10.5194/amt-14-455-2021>.

773 Levelt, P., Van den Oord, G., Dobber, M., Malkki, A., Visser, H., De Vries, J., et al. (2006). The ozone monitoring
774 instrument, *IEEE Transactions on Geosci, and Remote Sensing*, 44(5), 1093-1101.

775 Levelt, P. F., Joiner, J., Tamminen, J., Veefkind, J. P., Bhartia, P. K., Zweers, D. C. S. et al. (2018) The ozone monitoring
776 instrument: Overview of 14 years in space, *Atmospheric Chemistry and Physics*, 18(8):5699–5745,
777 <https://doi.org/10.5194/acp-18-5699-2018>.

778 Luftblick (2019a) Fiducial Reference Measurements for Air Quality, available at: [https://www.pandonia-global-](https://www.pandonia-global-network.org/wp-content/uploads/2021/01/LuftBlick_FRM4AQ_InstrumentChangeUpgrade_RP_2019002_v4.pdf)
779 [network.org/wp-content/uploads/2021/01/LuftBlick_FRM4AQ_InstrumentChangeUpgrade_RP_2019002_v4.pdf](https://www.pandonia-global-network.org/wp-content/uploads/2021/01/LuftBlick_FRM4AQ_InstrumentChangeUpgrade_RP_2019002_v4.pdf) (last
780 access: 15 March 2021).

781 Luftblick (2019b) Fiducial Reference Measurements for Air Quality TN on Data Quality Flagging Generic
782 Procedure Evolution, available at: [https://www.pandonia-global-network.org/wp-](https://www.pandonia-global-network.org/wp-content/uploads/2022/02/LuftBlick_FRM4AQ_DataQualityFlaggingGenericProcedureEvolution_TN_2019008_v5.pdf)
783 [content/uploads/2022/02/LuftBlick_FRM4AQ_DataQualityFlaggingGenericProcedureEvolution_TN_2019008_v5.pdf](https://www.pandonia-global-network.org/wp-content/uploads/2022/02/LuftBlick_FRM4AQ_DataQualityFlaggingGenericProcedureEvolution_TN_2019008_v5.pdf)
784 (last access: 15 March 2021).

785 Luftblick (2021) Pandonia Global Network Data Products Readme Document Version 1.8-3, available at:
786 https://www.pandonia-global-network.org/wp-content/uploads/2021/01/PGN_DataProducts_Readme_v1-8-3.pdf (last
787 access: 15 March 2021)

788 Luftblick (2022) [https://www.pandonia-global-network.org/wp-](https://www.pandonia-global-network.org/wp-content/uploads/2022/08/LuftBlick_FRM4AQ_NewAlgorithmPlan-ATBD_RP_2019005_v7.pdf)
789 [content/uploads/2022/08/LuftBlick_FRM4AQ_NewAlgorithmPlan-ATBD_RP_2019005_v7.pdf](https://www.pandonia-global-network.org/wp-content/uploads/2022/08/LuftBlick_FRM4AQ_NewAlgorithmPlan-ATBD_RP_2019005_v7.pdf)

790 Martins, D. K., Stauffer, R. M., Thompson, A. M., Knepp, T. N., Pippin, M. (2012), Surface ozone at a coastal suburban
791 site in 2009 and 2010: Relationships to chemical and meteorological processes, *Journal of Geophysical Research*, 117,
792 D05306, <https://doi.org/10.1029/2011JD016828>.

793 Martins, D. K., Najjar, R. G., Tzortziou, M., Abuhassan, N., Thompson, A.M., and D. E. Kollonige (2016), Spatial and
794 temporal variability of ground and satellite column measurements of NO₂ and O₃ over the Atlantic ocean during the
795 Deposition of Atmospheric Nitrogen to Coastal Ecosystems Experiment (DANCE), *Journal of Geophysical Research*,
796 121(23), <https://doi.org/10.1002/2016JD024998>.

797 NASA/LARC/SD/ASDC. (2022a). SCOAPE Ground Site Data [Data set]. NASA Langley Atmospheric Science Data
798 Center DAAC. Retrieved from https://doi.org/10.5067/ASDC/SUBORBITAL/SCOAPE_Ground_Data_1.

799 NASA/LARC/SD/ASDC. (2022b). SCOAPE R/V Point Sur Data [Data set]. NASA Langley Atmospheric Science Data
800 Center DAAC. Retrieved from https://doi.org/10.5067/ASDC/SUBORBITAL/SCOAPE_RVPointSur_Data_1.

801 NASA/LARC/SD/ASDC. (2022c). SCOAPE Pandora Column Observations [Data set]. NASA Langley Atmospheric
802 Science Data Center DAAC. Retrieved from
803 https://doi.org/10.5067/ASDC/SUBORBITAL/SCOAPE_Pandora_Data_1.

804 NASA/LARC/SD/ASDC. (2022d). SCOAPE Balloon and Ozonesondes Data [Data set]. NASA Langley Atmospheric
805 Science Data Center DAAC. Retrieved from https://doi.org/10.5067/ASDC/SUBORBITAL/SCOAPE_Sondes_Data_1.

806 Naval Research Laboratory and the University of North Dakota/MODIS Adaptive Processing System (MODAPS). (2017).
807 MODIS/Terra Aqua value-added Aerosol Optical Depth (MCDAODHD) [Dataset]. NASA Worldview Earthdata.
808 Retrieved from <https://worldview.earthdata.nasa.gov> and <http://doi.org/10.5067/MODIS/MCDAODHD.NRT.061>.

809 Nowlan, C. R., Liu, X., Leitch, J. W., Chance, K., Gonzalez, A. G., Liu, C., et al. (2016) Nitrogen dioxide observations
810 from the Geostationary Trace gas and Aerosol Sensor Optimization (GeoTASO) airborne instrument: Retrieval
811 algorithm and measurements during DISCOVER-AQ Texas 2013, *Atmospheric Measurement Techniques*, 9,
812 2647–2668, <https://doi.org/10.5194/amt-9-2647-2016>.

813 Petropavlovskikh, I., Ray, E., Davis, S. M., Rosenlof, K., Manney, G., Shetter, R., Hall, B., et al. (2010) Low ozone
814 bubbles observed in the tropical tropopause layer during the TC4 campaign in 2007, *Journal of Geophysical*
815 *Research*, 115, D00J16, <https://doi.org/10.1029/2009JD012804>.

816 Pipers, A. J. M., Boersma, K. F., Kroon, M., Hains, J. C., Van Roozendaal, M., Wittrock, F., et al. (2012) The Cabauw
817 Intercomparison campaign for Nitrogen Dioxide measuring Instruments (CINDI): Design, execution, and early results,
818 *Atmospheric Measurement Technology*, 457–485, <https://doi.org/10.5194/amt-5-457-2012>.

819 Platt, U. and Stutz, J. (2008) *Differential Optical Absorption Spectroscopy Principles and Applications*. Springer-Verlag.
820 <http://www.springer.com/environment/environmental+engineering+and+physics/book/978-3-540-21193-8>

821 Reed, A. J., Thompson, A. M., Kollonige, D. E., Martins, D. K., Tzortziou, M. A., Herman, J. R., Berkoff, T. A.,
822 Abuhassan, N. K., and A. Cede (2015), Effects of local meteorology and aerosols on ozone and nitrogen dioxide
823 retrievals from OMI and Pandora spectrometers in Maryland, USA during DISCOVER-AQ 2011, *J Atmos. Chem.*,
824 72(3-4), 455-482, <https://doi.org/10.1007/s10874-013-9254-9>.

825 Robinson, J., Kotsakis, A., Santos, F., Swap, R. J., Knowland, K. E., Labow, G., et al. (2020) Using networked Pandora
826 observations to capture spatiotemporal changes in total column ozone associated with stratosphere-to-troposphere
827 transport, *Atmospheric Research*, <https://doi.org/10.1016/j.atmosres.2020.104872>

828 Russell, A.R., Valin, L. C., and R. C. Cohen (2012). Trends in OMI NO₂ observations over the United States: effects of
829 emission control technology and the economic recession, *Atmos. Chem. Phys.*, 12, 12197–12209,
830 <https://doi.org/10.5194/acp-12-12197-2012>.

831 Schroeder, W., Giglio, L. (2017). VIIRS/NPP Thermal Anomalies/Fire 6-Min L2 Swath 750m V001 [Data set]. NASA
832 Worldview Earthdata. Retrieved from <https://worldview.earthdata.nasa.gov> and
833 <https://doi.org/10.5067/VIIRS/VNP14.001>.

834 Spinei, E. Tiefengraber, M., Müller, M., Gebetsberger, M., Cede, A., Valin, L., et al. (2021) Effect of polyoxymethylene
835 (POM-H Delrin) off-gassing within the Pandora head sensor on direct-sun and multi-axis formaldehyde column
836 measurements in 2016–2019, *Atmos. Meas. Tech.*, 14, 647–663. <https://doi.org/10.5194/amt-14-647-2021>

837 Stanier, C.O., Pierce, R.B., Abdi-Oskouei, M., Adelman, Z.E., Al-Saadi, J., Alwe, H.D., et al. (2021) Overview of The lake
838 Michigan ozone study 2017, *Bulletin of the American Meteorological Society*, <https://doi.org/10.1175/BAMS-D-20-0061.1>.

839 Stein, A. F., Draxler, R. R., Rolph, G. D., Stunder, B. J. B., Cohen, M. D., and F. Ngan (2015). NOAA's hysplit
840 atmospheric transport and dispersion modeling system. *Bulletin of the American Meteorological Society*, 96(12), 2059-
841 2077, <https://doi.org/10.1175/BAMS-D-14-00110.1>.

842 Sullivan, J. T., Dreessen, J., Berkoff, T., Delgado, R., Ren, X., Aburn, G., Jr. (2020) OWLETS -2: An Enhanced Monitoring
843 Strategy Directly within the Chesapeake Bay, *EM Magazine* (Air and Waste Management Assn), Oct 2020.

844 Sullivan, J. T., Berkoff, T., Gronoff, G., Knepp, T., Pippin, M., Allen, D., et al. (2018) The Ozone Water-Land
845 Environmental Transition Study (OWLETS): An innovative strategy for understanding Chesapeake Bay pollution
846 events, *Bulletin of the American Meteorological Society*, <https://doi.org/10.1175/BAMS-D-18-0025>.

847 Tack, F., Merlaud, A., Meier, A. C., Vlemmix, T., Ruhtz, T., Iordache, M.-D., Ge, X., et al. (2019) Intercomparison of four
848 airborne imaging DOAS systems for tropospheric NO₂ mapping – the AROMAPEX campaign, *Atmospheric*
849 *Measurement Techniques*, 12, 211–236, <https://doi.org/10.5194/amt-12-211-2019>, 2019

850 Thompson, A. M. (2020) Evaluation of NASA's remote-sensing capabilities in coastal environments. 49 p. OCS Study
851 BOEM 2020-047. https://espis.boem.gov/final%20reports/BOEM_2020-047.pdf.

852 Thompson, A. M., Doddridge, B. G., Witte, J. C., Hudson, R. D., Luke, W. T., Johnson, J. E., et al. (2000) A tropical
853 Atlantic paradox: Shipboard and satellite views of a tropospheric ozone maximum and wave-one in January-February
854 1999, *Geophysical Research Letters*, 27, 3317-3320, <https://doi.org/10.1029/1999GL011273>.

855 Thompson, A. M., MacFarlane, A.M., Morris, G. A., Yorks, J. E., Miller, S. K., Taubman, B. F., et al. (2010) Convective
856 and wave signatures in ozone profiles over the equatorial Americas: Views from TC4 (2007) and SHADOZ, *Journal of*
857 *Geophysical Research: Atmospheres*, 115, D00J23, <https://doi.org/10.1029/2009JD012909>.

858 Thompson, A. M., Miller, S. K., Tilmes, S., Kollonige, D. W., Witte, J. C., Oltmans, S. J., et al. (2012) Southern
859 Hemisphere Additional Ozonesondes (SHADOZ) ozone climatology (2005-2009): Tropospheric and tropical
860 tropopause layer (TTL) profiles with comparisons to OMI-based ozone products. *Journal Geophysical Research*, 117,
861 D23301, <https://doi.org/10.1029/2010JD016911>.

862 Thompson, A.M., Stauffer, R.M., Boyle, T.P.; Kollonige, D.E., Miyazaki, K., Tzortziou, M. A., et al. (2019a) Comparison
863 of near-surface NO₂ pollution with Pandora total column NO₂ during the Korea-United States Ocean Color (KORUS
864 OC) campaign, 2019, *Journal of Geophysical Research*, 124, <https://doi.org/10.1029/2019JD030765>.

865 Thompson, A. M., Smit, H. G. J., Witte, J. C., Stauffer, R. M., Johnson, B. J., Morris, G. A., et al. (2019b) Ozonesonde
866 Quality Assurance: The JOSIE-SHADOZ (2017) Experience, *Bulletin of the American Meteorological Society*,
867 <https://doi.org/10.1175/BAMS-17-0311>.

868 Thompson, A. M., Kollonige, D. E., Stauffer, R.M., Abuhassan, N., Kotsakis, A. E., Swap, R. J., and Wecht, H. E. (2020)
869 Satellite and shipboard views of air quality along the Louisiana coast: The 2019 SCOAPE (Satellite Coastal and
870 Oceanic Atmospheric Pollution Experiment) cruise, *EM Magazine* (Air and Waste Management Assn), Oct 2020.

871

872 Tirpitz, J.-L., Frieß, U., Hendrick, F., Alberti, C., Allaart, M., Apituley, A., et al. (2021). Intercomparison of MAX-
873 DOAS vertical profile retrieval algorithms: studies on field data from the CINDI-2 campaign, *Atmos. Meas.*
874 *Tech.*, 14, 1–35. <https://doi.org/10.5194/amt-14-1-2021>

875 Tong, D. Q., Lamsal, L., Pan, L., Ding, C., Kim, H., Lee, P., et al. (2015) Long-term NO_x trends over large cities in the
876 United States during the great recession: Comparison of satellite retrievals, ground observations, and emission
877 inventories, *Atmos. Environ.*, 107, 70–84, <https://doi.org/10.1016/j.atmosenv.2015.01.035>.

878 Tzortziou, M., Herman, J. R., Loughner, C. P., Cede, A., Abuhassan, N., and Naik, S. (2015a). Spatial and temporal
879 variability of ozone and nitrogen dioxide over a major urban estuarine ecosystem, *J. Atmos. Chem.*,
880 <https://doi.org/10.1007/s10874-013-9255-8>.

881 Tzortziou, M., Thompson, A. M., and J. Herman (2015b), Dynamics of atmospheric trace gases and aerosols in Korean
882 coastal waters: Impacts on ocean color atmospheric correction and surface air pollution studies (NASA Project
883 Description, Grant # NNX16AD60G, PI: Tzortziou).

884 Tzortziou, M., Parker, O., Lamb, B., Herman, J., Lamsal, L., Stauffer, R., and Abuhassan, N. (2018). Atmospheric trace gas
885 (NO₂ and O₃) variability in Korean coastal waters, implications for remote sensing of coastal ocean color dynamics,
886 *Remote Sens.*, 10, <https://doi.org/10.3390/rs10101587>.

887 van Geffen, J. H. G. M., Eskes, H. J., Boersma, K. F., Maasakkers, J. D., Veefkind, J. P. (2018). TROPOMI ATBD of the
888 total and tropospheric NO₂ data products (issue 1.2.0). Royal Netherlands Meteorological Institute (KNMI), De Bilt, the
889 Netherlands, [http://www.tropomi.eu/sites/default/files/files/publicS5P-KNMI-L2-0005-RP-ATBD_NO2_data_products-
890 20190206_v140.pdf](http://www.tropomi.eu/sites/default/files/files/publicS5P-KNMI-L2-0005-RP-ATBD_NO2_data_products-20190206_v140.pdf).

891 van Geffen, J., Eskes, H., Compennolle, S., Pinardi, G., Verhoelst, T., et al. (2022) Sentinel-5P TROPOMI NO₂ retrieval:
892 impact of version v2.2 improvements and comparisons with OMI and ground-based data, *Atmospheric Measurement*
893 *Techniques*, 15, 2037–2060, <https://doi.org/10.5194/amt-15-2037-2022>.

894 Veefkind, J., Aben, I., McMullan, K., Forster, H., de Vries, J., Otter, G., et al. (2012). TROPOMI on the ESA Sentinel-5
895 Precursor: A GMES mission for global observations of the atmospheric composition for climate, air quality and ozone
896 layer applications. *Remote Sens. of Environ.*, 120, 70–83, <https://doi.org/10.1016/j.rse.2011.09.027>.

897 Verhoelst, T., Compennolle, S., Pinardi, G., Lambert, J.-C., Eskes, H. J., Eichmann, K.-U., et al. (2021) Ground-based
898 validation of the Copernicus Sentinel-5P TROPOMI NO₂ measurements with the NDACC ZSL-DOAS, MAX-DOAS
899 and Pandora global networks, *Atmos. Meas. Tech.*, 14, 481–510. <https://doi.org/10.5194/amt-14-481-2021>

900 Wilson, D. R., Billings, R., Chang, S., Enoch, B., Do, H., Perez, H., Sellers, J. (2017) Year 2014 Gulfwide emissions
901 inventory study. US Dept. of the Interior, Bureau of Ocean Energy Management, Gulf of Mexico OCS Region, New
902 Orleans, LA. OCS Study BOEM 2017-044. 275 pp. [https://www.boem.gov/environment/environmental-studies/2014-
903 gulfwide-emission-inventory](https://www.boem.gov/environment/environmental-studies/2014-gulfwide-emission-inventory).

904 Wilson, D., Billings R., Chang, R., Do, B., Enoch, S., Perez, H., and Sellers, J. (2019) Year 2017 emissions inventory study.
905 New Orleans (LA): US Department of the Interior, Bureau of Ocean Energy Management. OCS Study BOEM 2019-
906 072. 231 p., https://espis.boem.gov/final%20reports/BOEM_2019-072.pdf.

907 Yacovitch, T., Daube, C., Herndon, S. (2020) Methane emissions from offshore oil and gas platforms in the Gulf of Mexico,
908 *Environ. Sci. Technol.* 2020, 54, 6, 3530–3538, <https://doi.org/10.1021/acs.est.9b07148>.

909 Yarnes, C. (2013), $\delta^{13}\text{C}$ and $\delta^2\text{H}$ measurement of methane from ecological and geological sources by gas
910 chromatography/combustion/ pyrolysis isotope-ratio mass spectrometry, *Rapid Commun. Mass Spectrom.*, 27, 1036–
911 1044, <https://doi.org/10.1002/rcm.6549>.

912
913
914
915
916
917
918
919
920
921
922
923
924
925
926
927
928
929

930 **Table 1.** List of relevant campaigns and experiments that preceded SCOAPE.
 931

Campaign (Year(s))	Geographic Location	Reference
CAPABLE (2009, 2010, 2011)	Hampton, VA	<i>Martins et al. (2012)</i> <i>Knepp et al. (2015)</i>
DISCOVER-AQ MD (2011)	Baltimore, MD -Washington, D.C.	<i>Reed et al. (2015)</i> <i>Tzortziou et al. (2015)</i>
DISCOVER-AQ TX (2013)	Houston, TX	<i>Flynn et al. (2014)</i> <i>Nowlan et al. (2016)</i> <i>Judd et al. (2019)</i>
DANCE (2014)	Atlantic Coast (DE-NC)	<i>Martins et al. (2016)</i> <i>Kollonige et al. (2018)</i>
KORUS-OC (2016)	Southern Korean peninsula	<i>Tzortziou et al., (2018)</i> <i>Thompson et al. (2019a)</i>
LMOS (2017)	Lake Michigan	<i>Adelman et al. (2020)</i> <i>Stanier et al. (2021)</i>
OWLETS (2017)	Hampton, VA; Lower Chesapeake Bay	<i>Sullivan et al. (2018)</i> <i>Gronoff et al. (2019)</i> <i>Dacic et al. (2020)</i>
OWLETS-2 (2018)	Baltimore, MD; Upper Chesapeake Bay	<i>Sullivan et al. (2020)</i> <i>Kotsakis et al. (2022)</i>
LISTOS (2018)	Long Island Sound, NY	<i>Judd et al. (2020)</i> <i>Karambelas et al. (2020)</i>

932

933 **Table 2.** Offshore instrumentation on R/V Point Sur during SCOAPE cruise.

Species	Instrument	Collaborator
NO₂ (and calibrator)	In situ (Teledyne API T500U CAPS)	NASA GSFC
Column NO₂	Pandora (PSI)	NASA GSFC (Swap*)
O₃	In situ (Thermo Fisher Scientific 49i UV Photometer) and Ozonesondes	NASA GSFC
Temperature, RH, etc.	Met system (Vaisala all-in one meteorological sensor)	<i>R/V Point Sur</i>
Aerosol (AOD) & O₃ columns	Microtops Columns	NASA GSFC
VOCs (plus CO & CH₄)	In situ canisters	UCI (Blake)
PBL height	Ceilometer (Lufft CHM 8k)	UMBC (Delgado)
Black carbon	Aethalometer (Magee Scientific RTA10 7-channel)	NIST (Conny)
CH₄, CO₂, H₂O	In situ (Picarro G-1301m)	GSFC (Kawa / Hanisco)

934 * Collaborators for loaned instruments in parentheses.

935 **Table 3.** Onshore instrumentation during SCOAPE cruise.

Species	Instrument	Collaborator
NO₂	In situ analyzer	NASA GSFC (Sullivan)

NO ₂	Mobile in situ (NO ₂ sonde)	KNMI (Stein-Zweers/den Hoed)
Column NO ₂	Pandora	NASA GSFC (Swap)
VOCs (plus CO & CH ₄)	In situ canisters	UCI (Blake)
PBL height	Ceilometer	U Houston (Flynn)

936
937
938
939

Table 4. AQ conditions from VOC can sample on 16 May near shallow-water platform at (28.9795°, -91.4760°).

VOC Species	Cruise Median	16 May Plume Can	Notes
CH ₄ (ppmv)	1.96	5.71	Deepwater platforms flare this off
CO ₂ (ppmv)	415	418	No combustion, likely just leaky pipes
Ethane (ppbv)	2.1	145	C ₂ H ₆ ; second largest component of fossil gas after CH ₄
Propane (ppbv)	0.7	90.1	C ₃ H ₈ ; byproduct of fossil gas processing
n-Butane (ppbv)	0.3	29.9	C ₄ H ₁₀ ; i-Butane had similar concentrations
Benzene (ppbv)	0.04	1.88	C ₆ H ₆ ; known carcinogen

940
941
942

Figure captions.

943
944
945
946
947
948
949
950
951
952
953

Figure 1. SCOAPE cruise track (black), with arrows indicating movements of *R/V Point Sur* in May 2019. Pandora calibrations were conducted at Cocodrie. Canister samples were coordinated with ship canister filling from locations in Louisiana depicted as red pins. Emissions shown for NO_x by Wilson et al. (2017, 2019) are BOEM’s publicly available estimates based on monthly reports of fuel usage by operators using the Gulfwide Offshore Activities Data System (GOADS). EPA emission factors for methane, VOC, SO₂, CO, CO₂, NO_x and particulate matter are used to convert the GOADS data into the values shown here. Sources of platform NO_x emissions include diesel engines and combustion flares. Figures 4, 9 and 10 illustrate trace gases from encounters with some of the named platforms here.

954
955
956
957
958
959
960
961
962

Figure 2. MERRA-2 meteorological reanalysis at 12 UTC (0600 Local Time) for four days (12-15 May 2019) that capture the transition from onshore flow, (a) and (b), to mostly offshore winds (c) and (d). Unpolluted, moister tropical air masses were sampled on 12 and 13 May with a transition to air parcels originating from the near-shore and more urban Louisiana coastal areas on 14 and 15 May. The *R/V Point Sur* cruise track is shown in cyan, with the location of the ship indicated by the red dot. MERRA-2 MSLP (black contours), 1000 hPa wind vectors (black arrows) and 1000 hPa specific humidity (colors) summarize the large-scale meteorological conditions encountered during the middle of the cruise.

963
964
965
966
967
968
969

Figure 3. OMI v4 effective cloud fraction over SCOAPE cruise region on (a) 13 May 2019 and (b) 15 May 2019 (Krotkov et al., 2019). Total Column (TC) NO₂ (DU) over SCOAPE cruise region from OMI v4 on (c) 13 May 2019 and (d) 15 May 2019 (Krotkov et al., 2019). TROPOMI v1.3 TC NO₂ (DU) for (e) 13 May 2019 and (f) 15 May 2019 (Copernicus Sentinel-5P, 2018). TROPOMI maps produced using the PAL retrieval for May 2019 differed from TROPOMI v1.3 by < 5% overwater. In (c) through (f) black open squares are the locations of the top 500 NO_x-emitting platforms from BOEM’s 2014 inventory (Wilson et al., 2017); white open squares mark

970 the same in (a) and (b). The gray solid line marks the *R/V Point Sur* cruise track. New Orleans,
971 Louisiana (NOLA), and Baton Rouge are indicated with open gray stars.

972
973 Figure 4. (a) Ozone mixing ratio (right scale) in ppbv with wind direction (left scale, in degrees)
974 measured on *R/V Point Sur* during May 2019 cruise (presented as 5-minute means); (b) NO₂
975 mixing ratio (left scale; 15-minute means) in ppbv with CO mixing ratio in ppbv from canister
976 samples taken along the *Point Sur* track. Trace-gas data retrieved from *NASA/LARC/SD/ASDC*
977 (2022b). Sampling locations (Figure 1) are as follows: 1 = vicinity of Mars/Olympus deepwater
978 platform complex; 2 = near Atlantis platform before 13 May wind shift (Figure 2); 3 = between
979 Marco Polo and Shenzi platforms after 13 May wind shift; 4 = near Brutus platform, VOC-
980 enriched plume detected; 5 = second encounter, vicinity of Mars/Olympus complex, 14 May,
981 plume detected. Note: Surface NO₂ values are higher than encounter [1] because the background
982 is more polluted on 14 May than on 12 May; 6 = near Petronius, second encounter (see elevated
983 methane, VOC in Figure 7, also Figures 9 and 10a); 7 = surrounded by numerous shallow water
984 platforms in western area, where VOC-enhanced plume detected (Table 4).

985
986 Figure 5. Ozonesonde profiles during SCOAPE, data downloaded from *NASA/LARC/SD/ASDC*
987 (2022d). Mixing ratios to 16 km are illustrated. Blue colors are concentrations associated with
988 tropical marine boundary layer. On 12-14 May ozone concentrations 20-30 ppbv above 10 km are
989 typical of air parcels in which deep convection introduced boundary layer air. From 15 to 17 May
990 layers with > 80 ppbv signify stratospheric influence. See Figure S7 where up to 14 May lower
991 ozone mixing ratios occur with higher humidity measured by the accompanying radiosondes.
992 From 15-17 May, from 4 to 16 km, the median relative humidity has fallen to < 10%.

993
994 Figure 6. Box and whisker panels for CH₄, CO, CO₂ and dimethylsulfide (DMS) before (left side
995 of each panel) and after 14 May (right side of each panel). Data were taken from
996 *NASA/LARC/SD/ASDC* (2022b). Sample numbers indicated at the top or bottom of each panel.
997 Red line denotes median values, blue box denotes 25th and 75th percentile, and whiskers (dashed
998 bars) are 95th percentile. Notches in the boxes indicate the 95% confidence interval of the median
999 values.

1000
1001 Figure 7. VOC canister observations of CH₄ isotope source signatures for ship (circles) and
1002 coastal (squares) measurements 11-19 May 2019. Colormap indicates ethane to methane ratios (%
1003 (ppb/ppb)) in the scatter plot (a) and map (b). Error bars show 1-sigma standard deviation.

1004
1005 Figure 8. HYSPLIT 12-hour ensemble back trajectories (*Stein et al.*, 2015) released at 50m (top
1006 panels; a-c) and 500m (lower panels; d-f) at the local times listed in each (12-14 May 2019) and
1007 driven by the NCEP Global Data Assimilation System (GDAS) at 0.5° resolution. Colors of the
1008 trajectories denote change in ensemble trajectories' release time (every 3 hours over 12-hour
1009 period).

1010
1011 Figure 9. Pandora diurnal cycle of TC NO₂ (data from *NASA/LARC/SD/ASDC*, 2022c) during the
1012 cruise period 11-17 May 2019 (color of lines denotes day of observation) with TROPOMI
1013 overpass values (diamonds in corresponding day of cruise color; *Copernicus Sentinel-5P*, 2018)
1014 and OMI v4 overpass values (triangles in corresponding day of cruise color; *Krotkov et al.*, 2019).
1015 Platform encounters labeled 1, 5 and 6, as described in Figure 4. Note that although 1 (12 May)
1016 and 5 (14 May) both correspond to sampling near the Mars/Olympus complex, TC NO₂ is lower

1017 for the earlier encounter because the background air with air parcels from the south (Figure 8a, d)
1018 is less polluted than with flows from the north and east (Figure 8c, f).

1019
1020 Figure 10. (a) Time series of TROPOMI, OMI v4, Pandora TC NO₂ and in situ NO₂ during
1021 SCOAPE cruise. Pandora TC NO₂ measurements and in situ data are time-matched 5-min
1022 averages. Location key same as Figures 1 and 9. (b) Pandora TC NO₂ along ship track (in gray),
1023 10-18 May 2019, during cruise. Blue squares mark locations of platforms that fall into the top 500
1024 NO_x emitters category according to the 2014 BOEM inventory (*Wilson et al.*, 2017). The cruise
1025 segment with cleaner air (south of 28.3°N; cf. Figures 4 and 5), was sampled prior to 14 May.
1026 Polluted air at and north of 28.5°N was sampled after 14 May.

1027
1028 Figure 11. Satellites vs. Pandora (Pan) 66 TC NO₂ on the *R/V Point Sur* during the cruise period
1029 11-17 May 2019 with OMI v3 (light blue circles), OMI v4 (blue triangles), and TROPOMI v1.3
1030 (cyan diamonds) readings referred to y-axis versus Pandora 66 on x-axis. Satellites vs. Pandora
1031 TC NO₂ at LUMCON 11-17 May 2019 with: OMI v3 versus Pandora 67 (light yellow circles) and
1032 68 (yellow circles) on the x-axis; OMI v4 versus Pandora 67 (dark green triangles) and 68 (green
1033 triangles) on the x-axis; and TROPOMI v1.3 versus Pandora 67 (gold diamonds) and 68 (tan
1034 diamonds) on the x-axis.
1035

Figure 1.

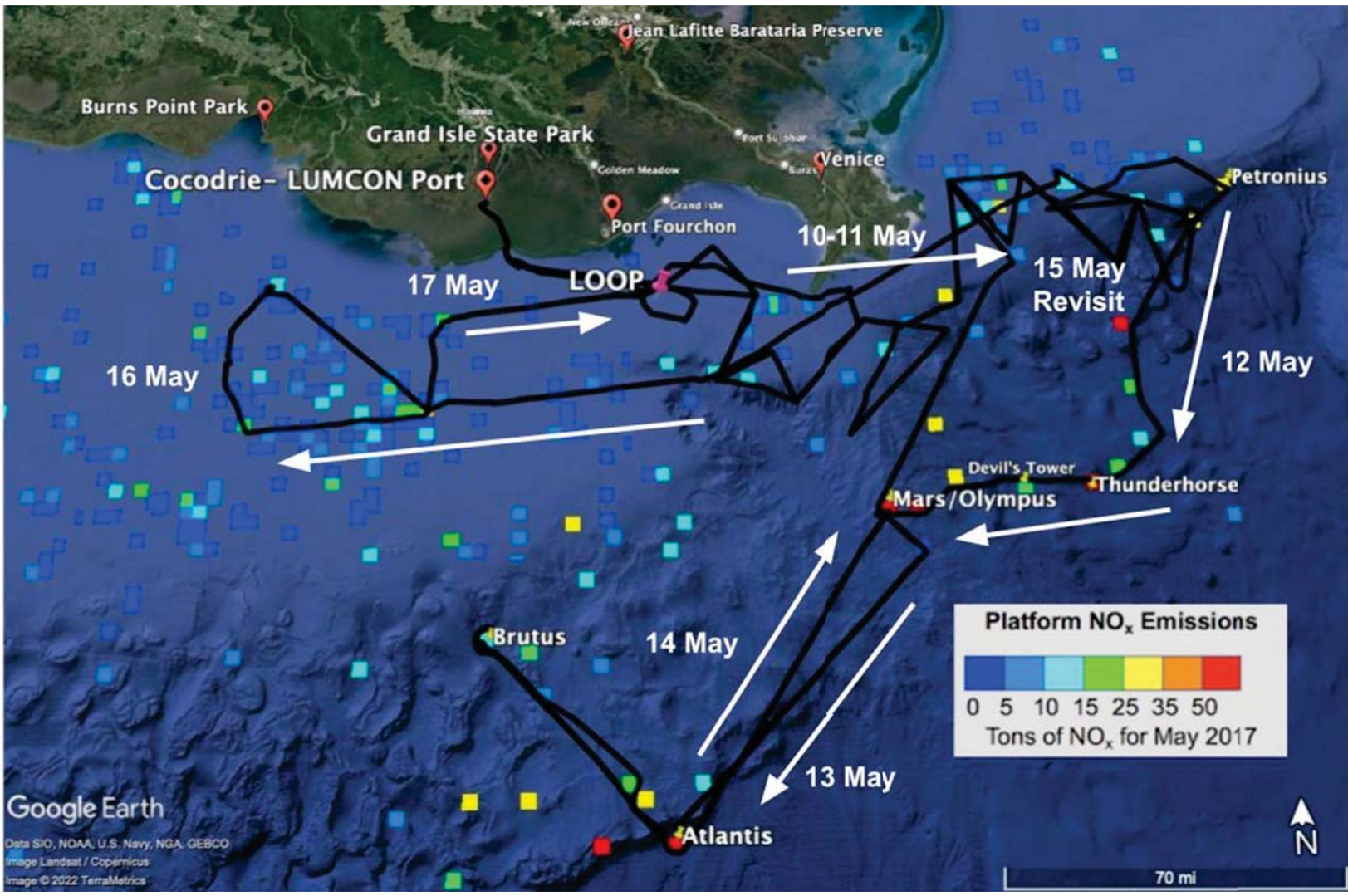


Figure 2.

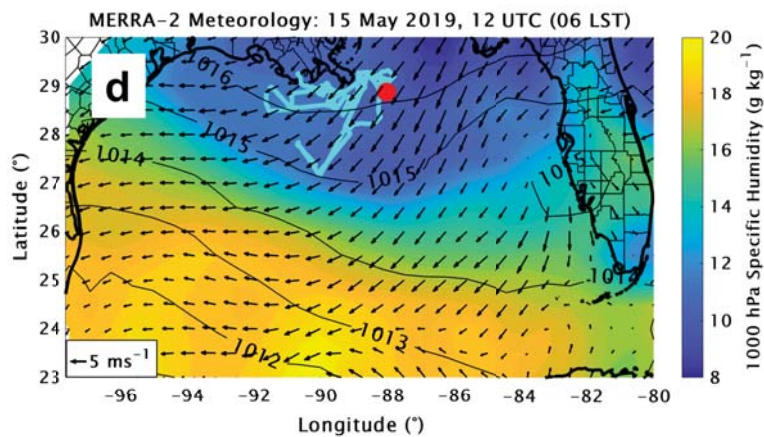
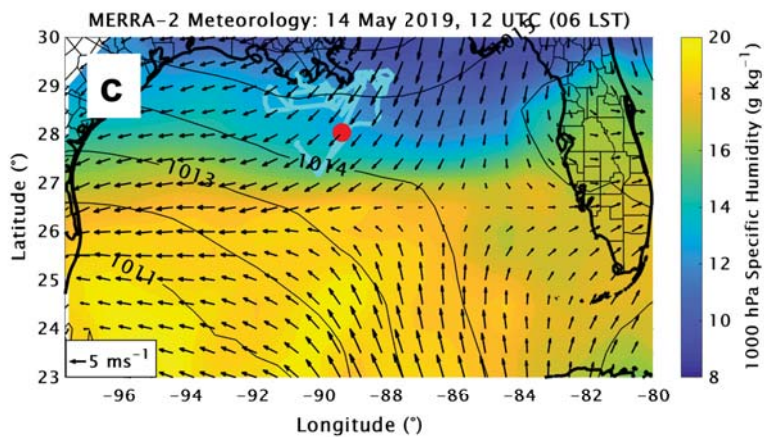
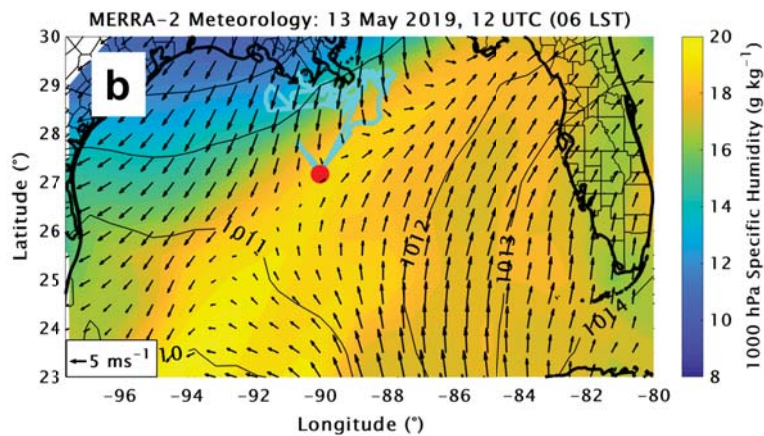
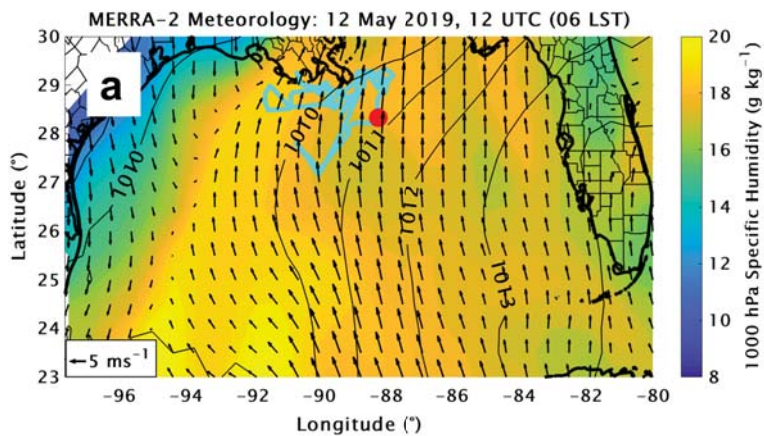


Figure 3.

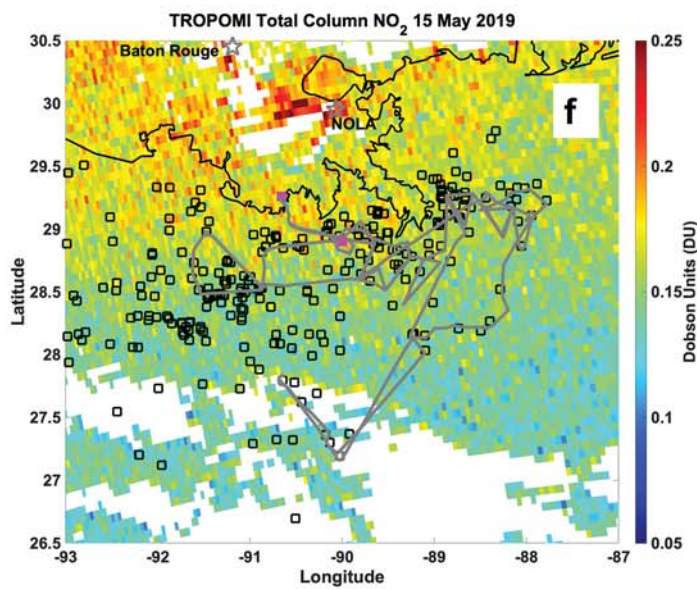
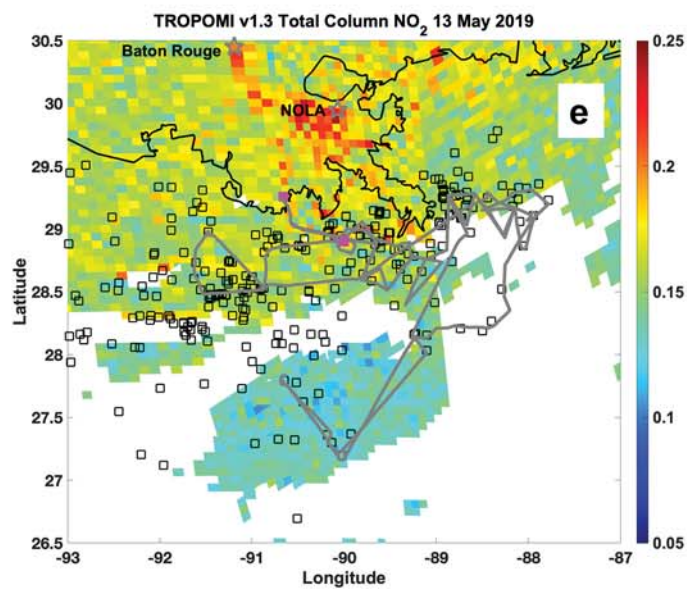
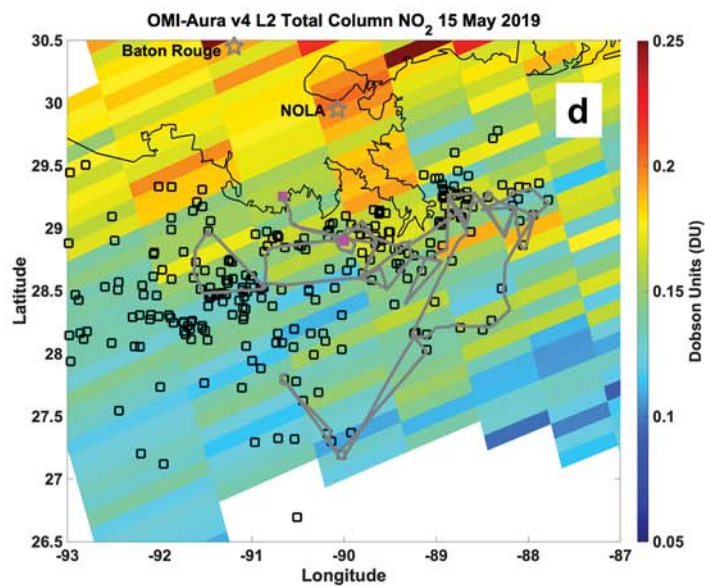
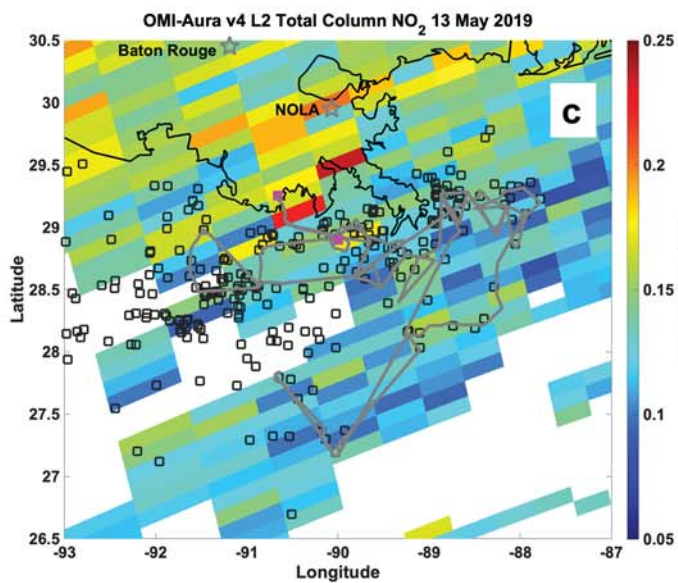
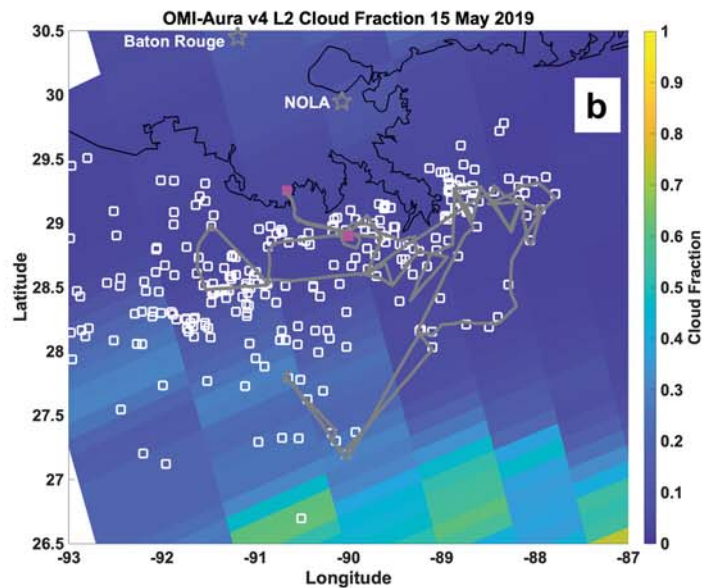
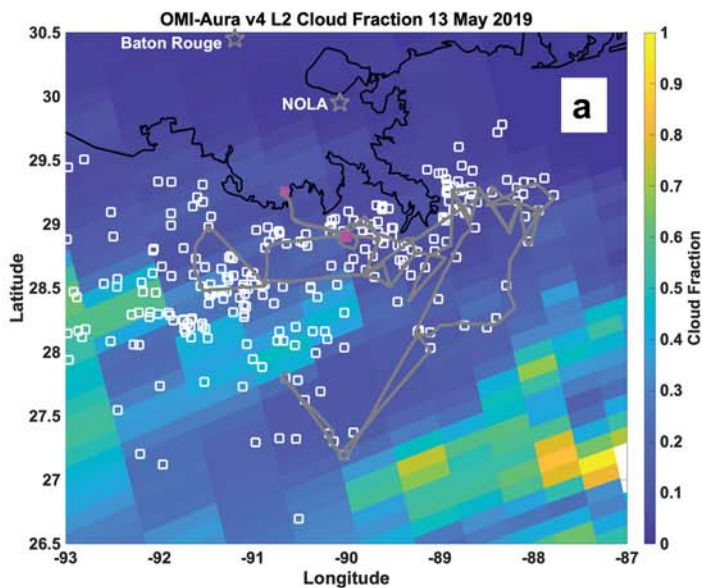


Figure 4.

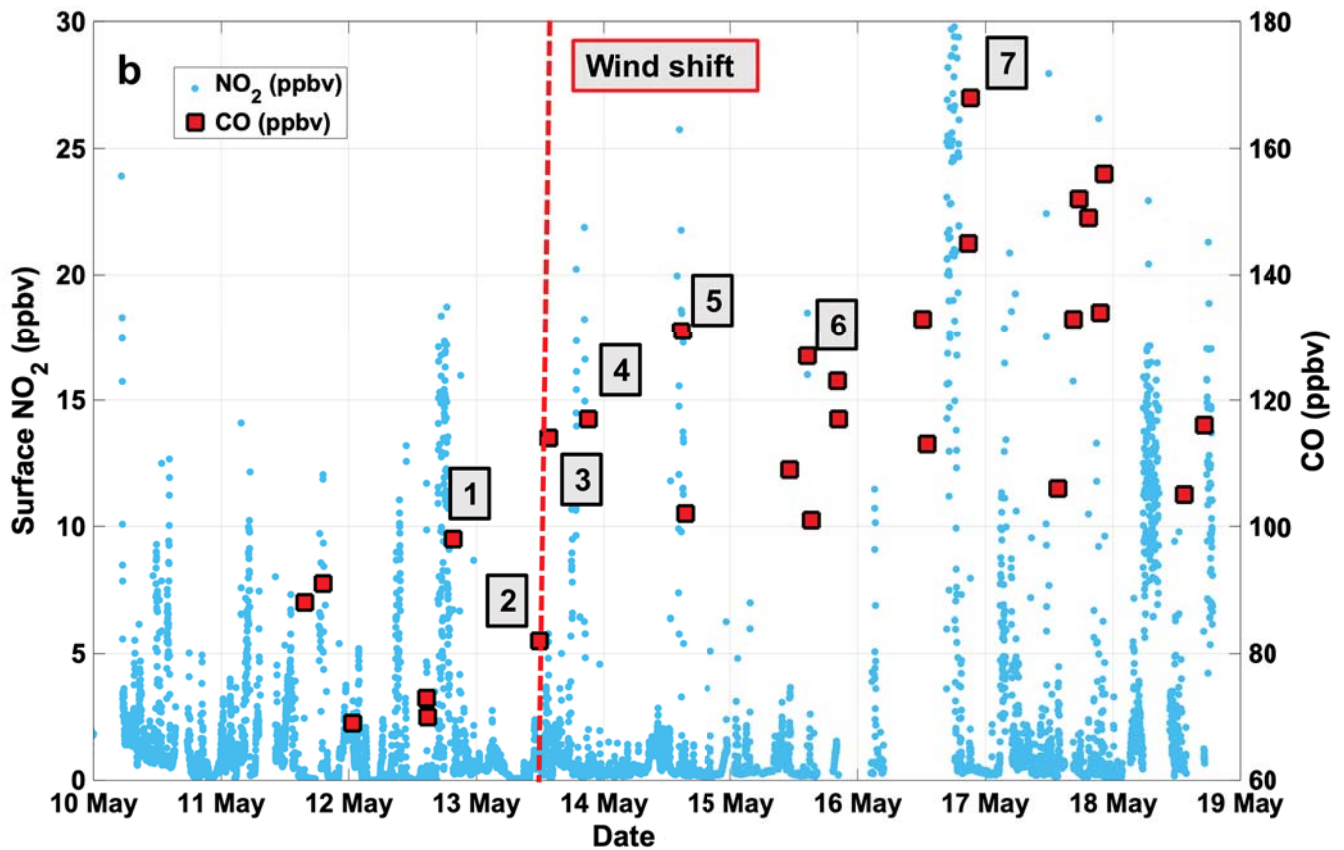
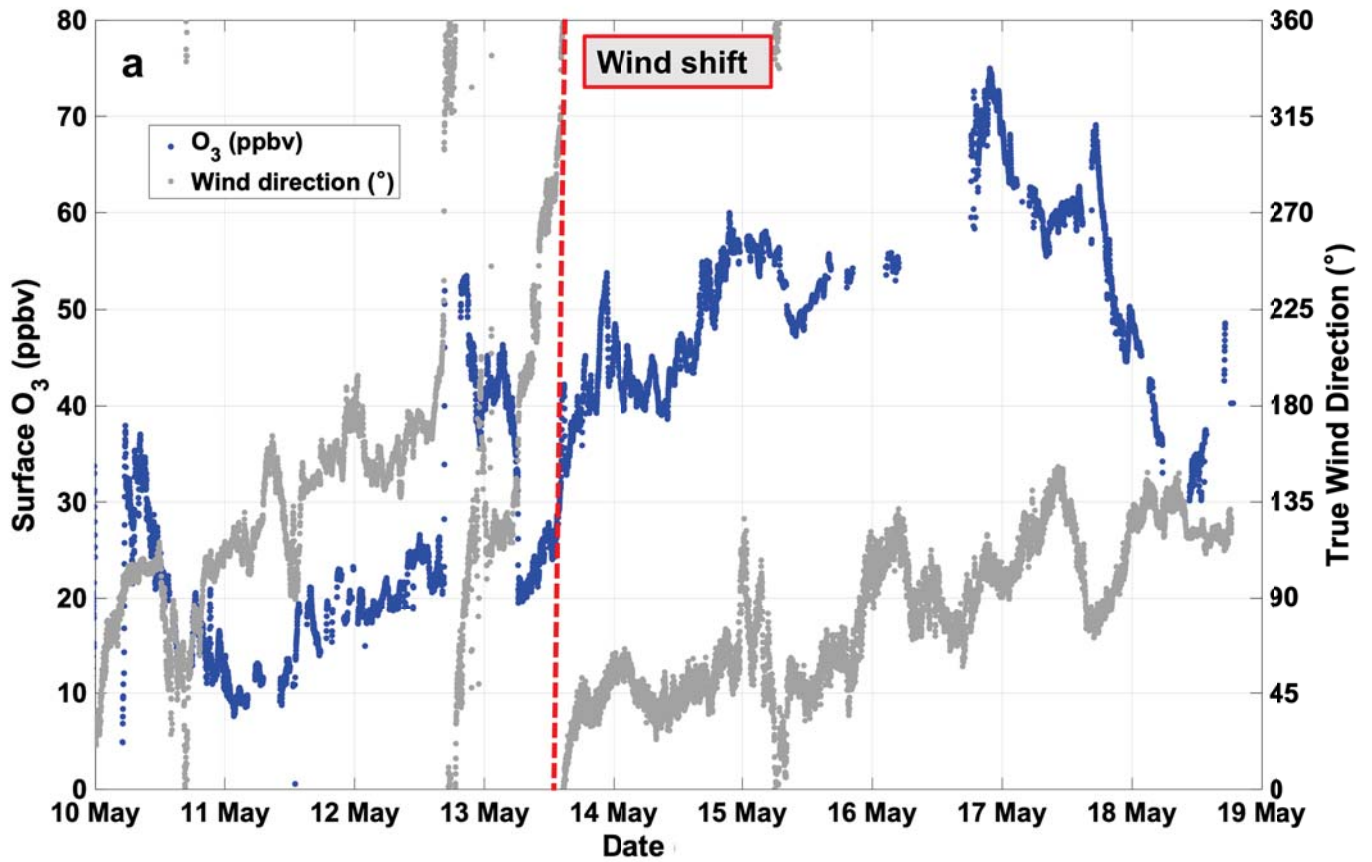


Figure 5.

Ozonesonde Profiles during SCOAPE

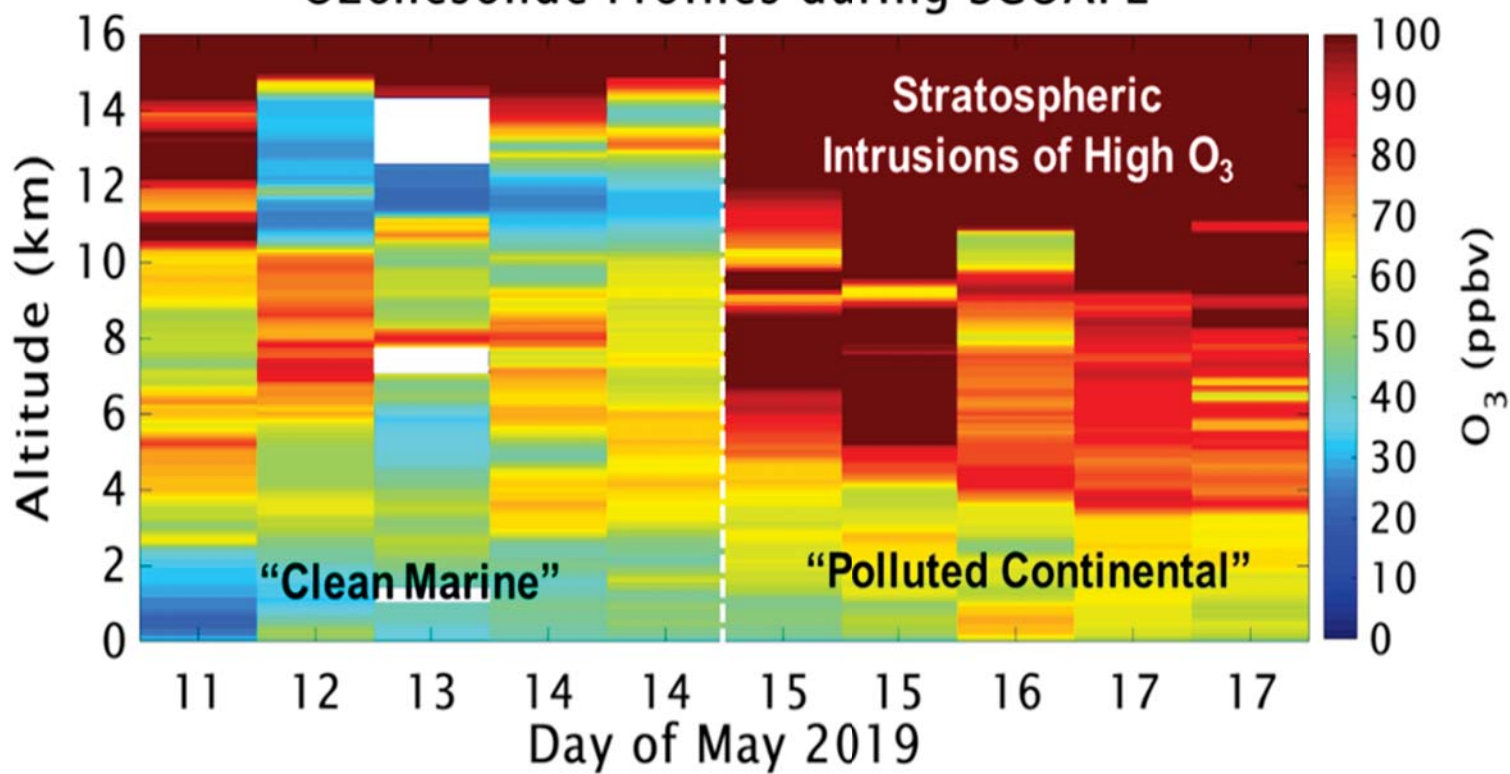


Figure 6.

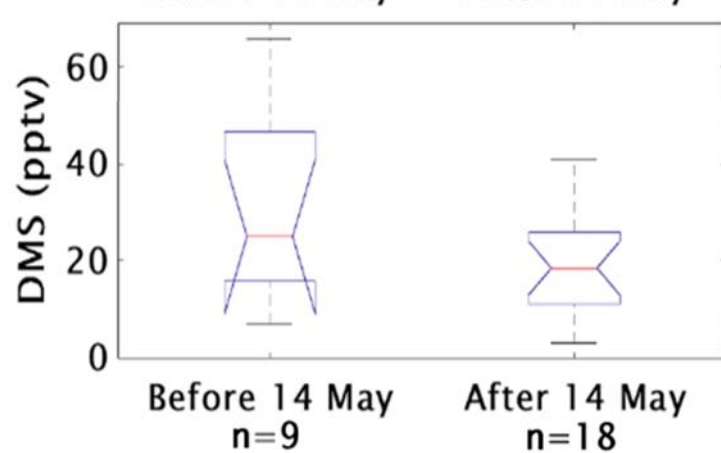
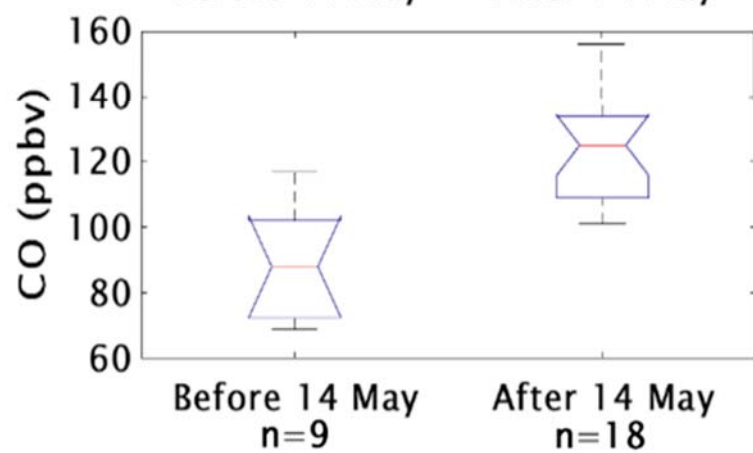
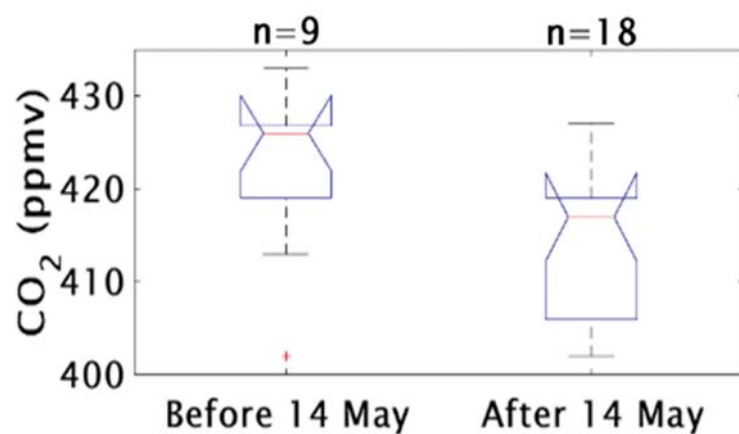
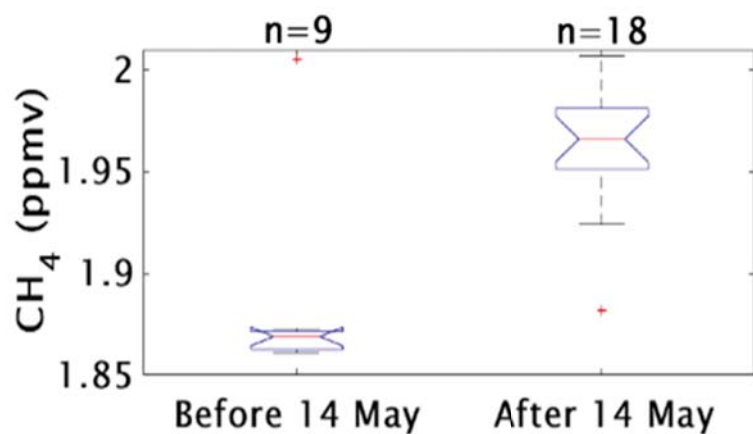


Figure 7.

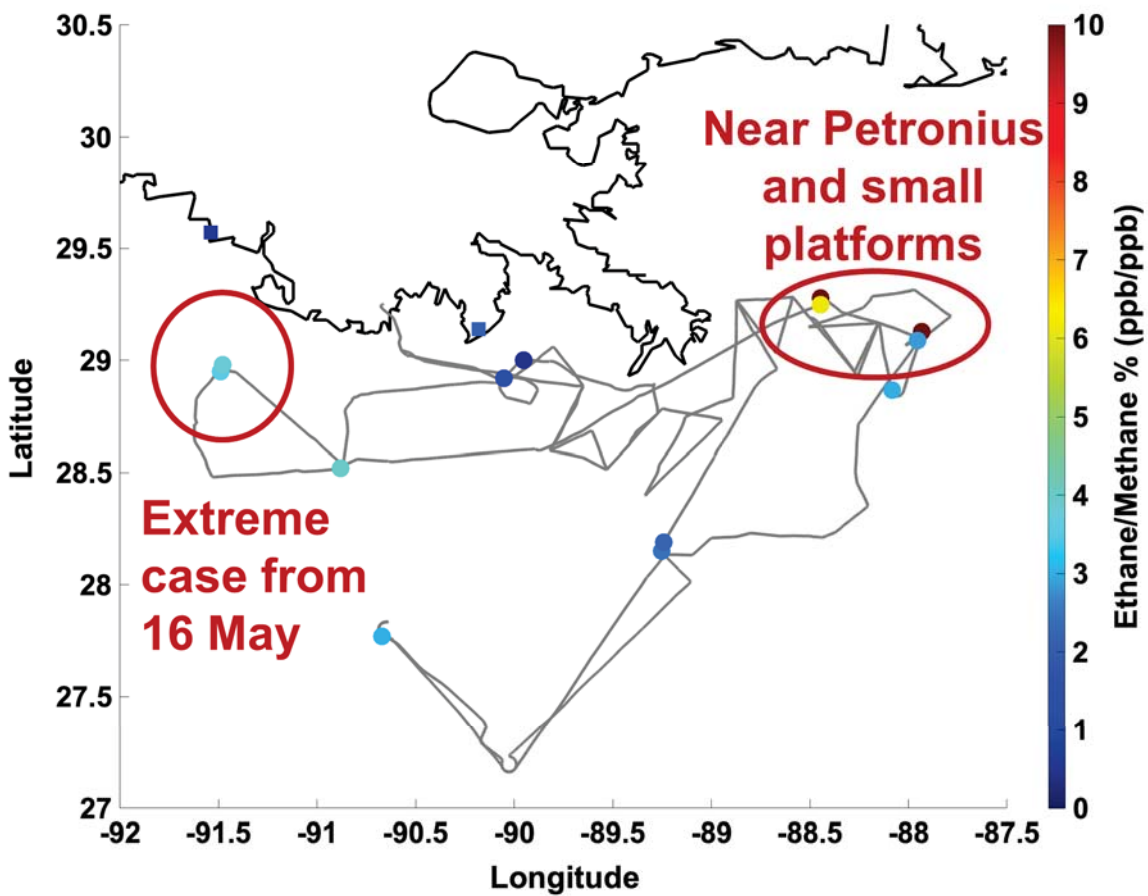
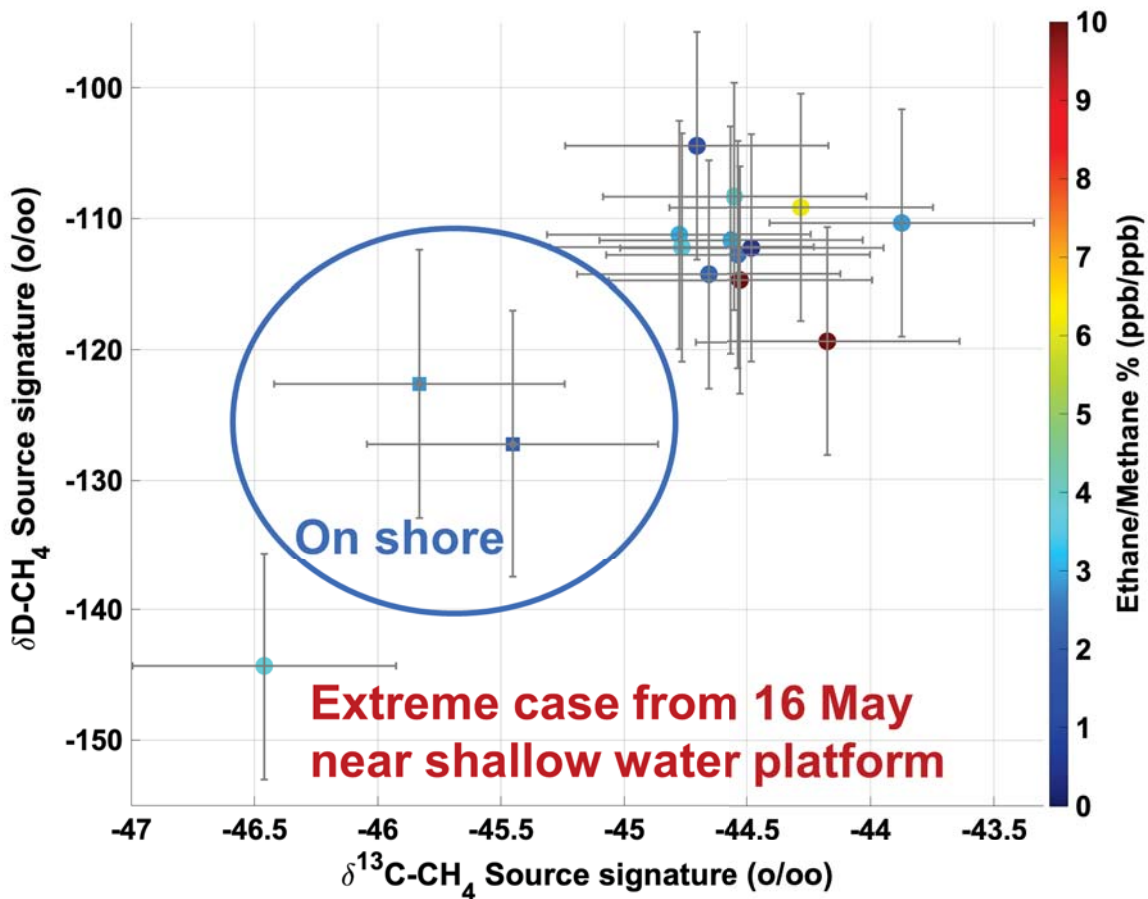


Figure 8.

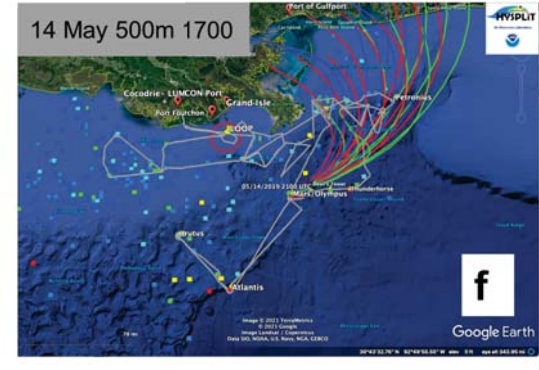
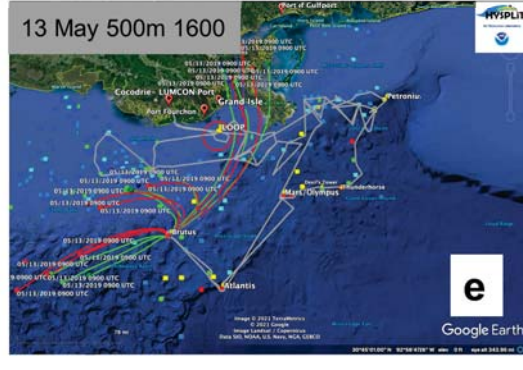
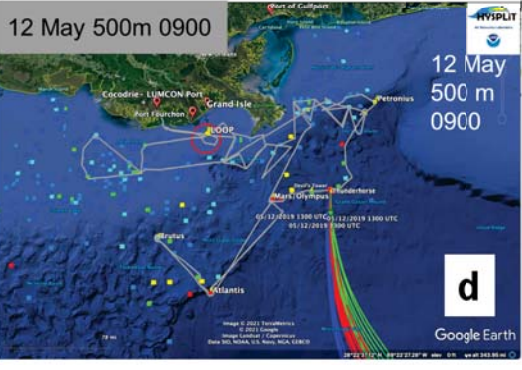
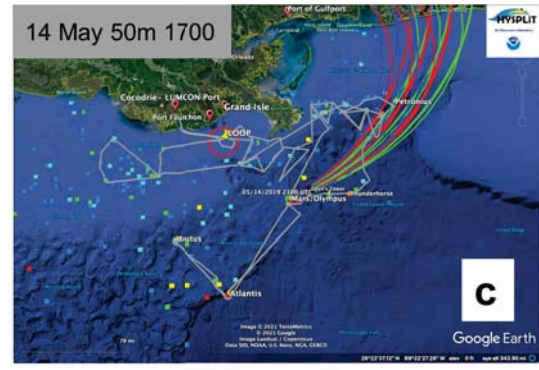
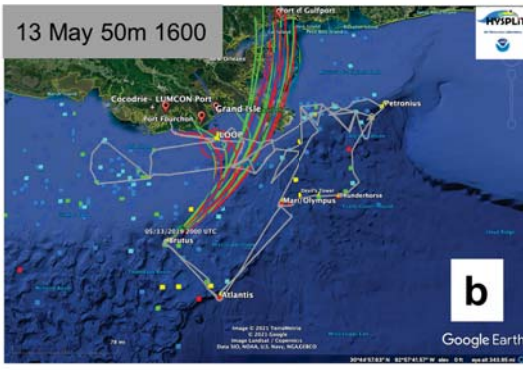
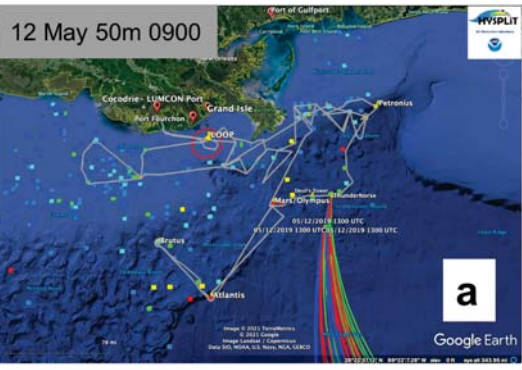


Figure 9.

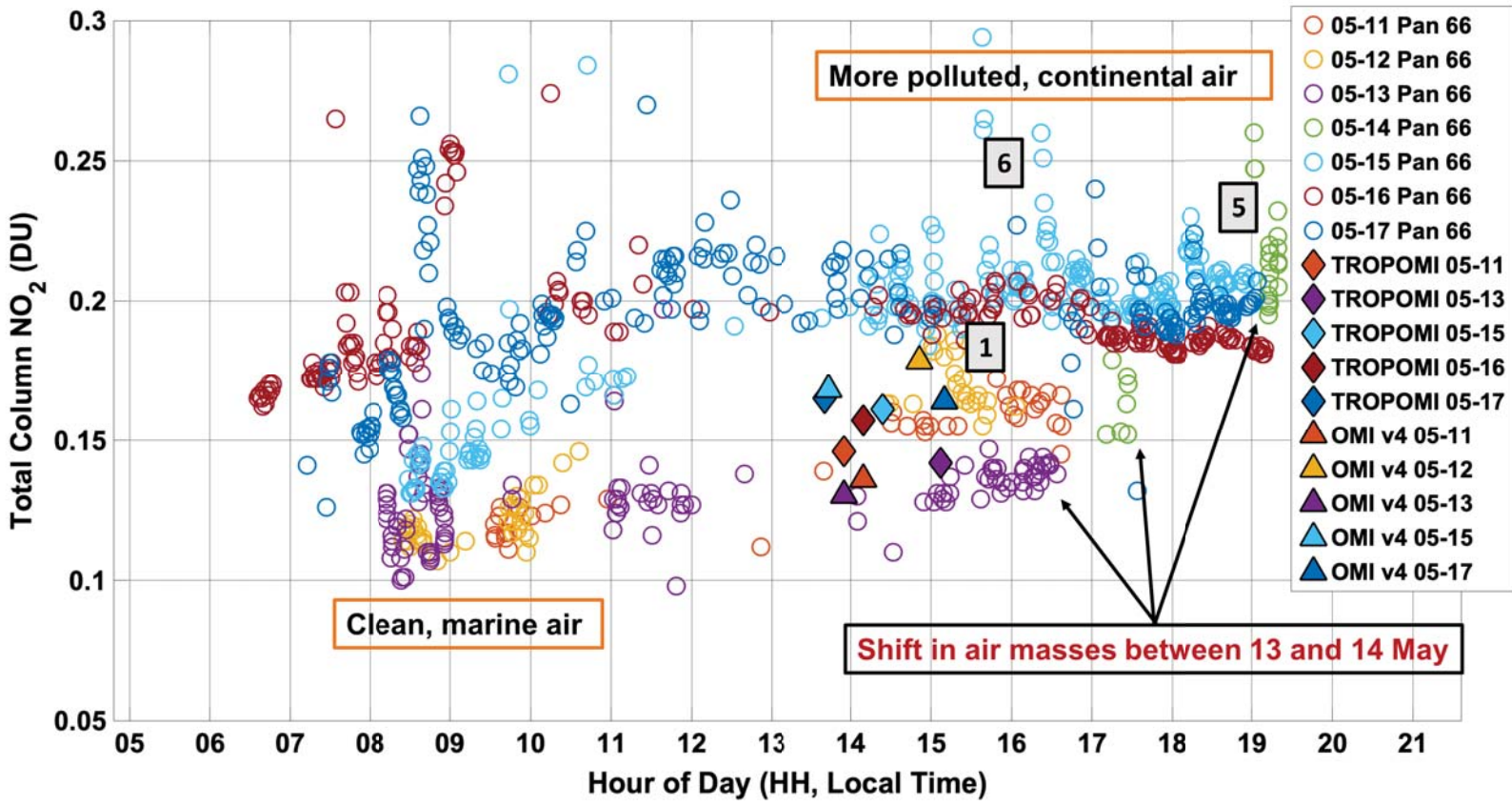


Figure 10.

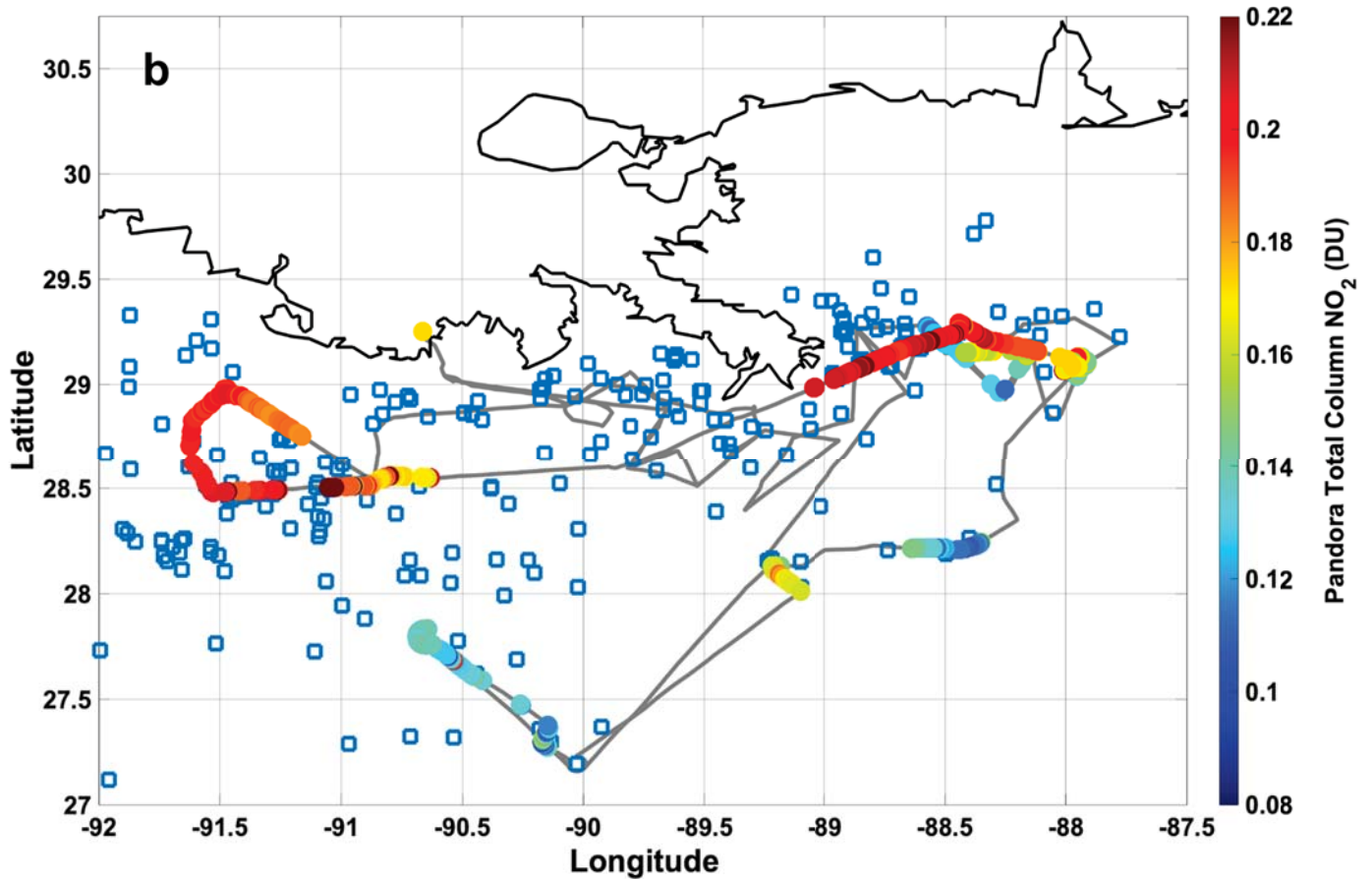
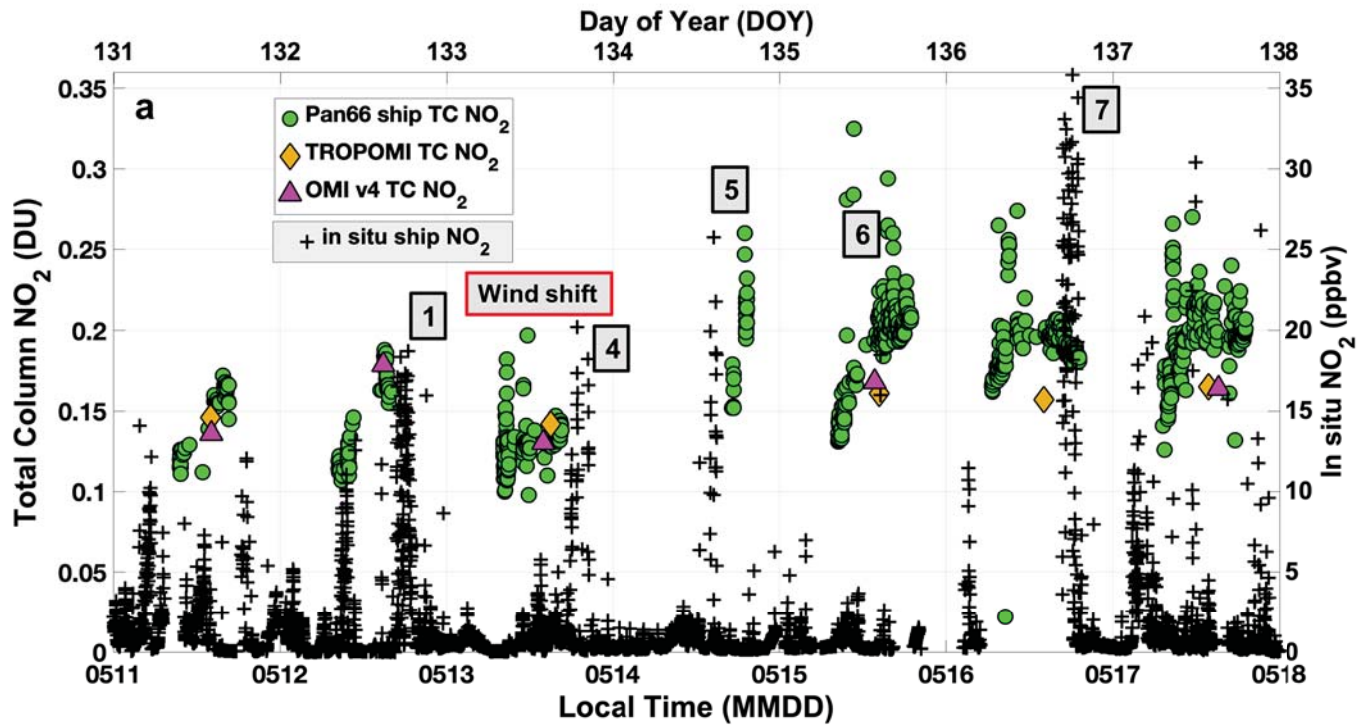
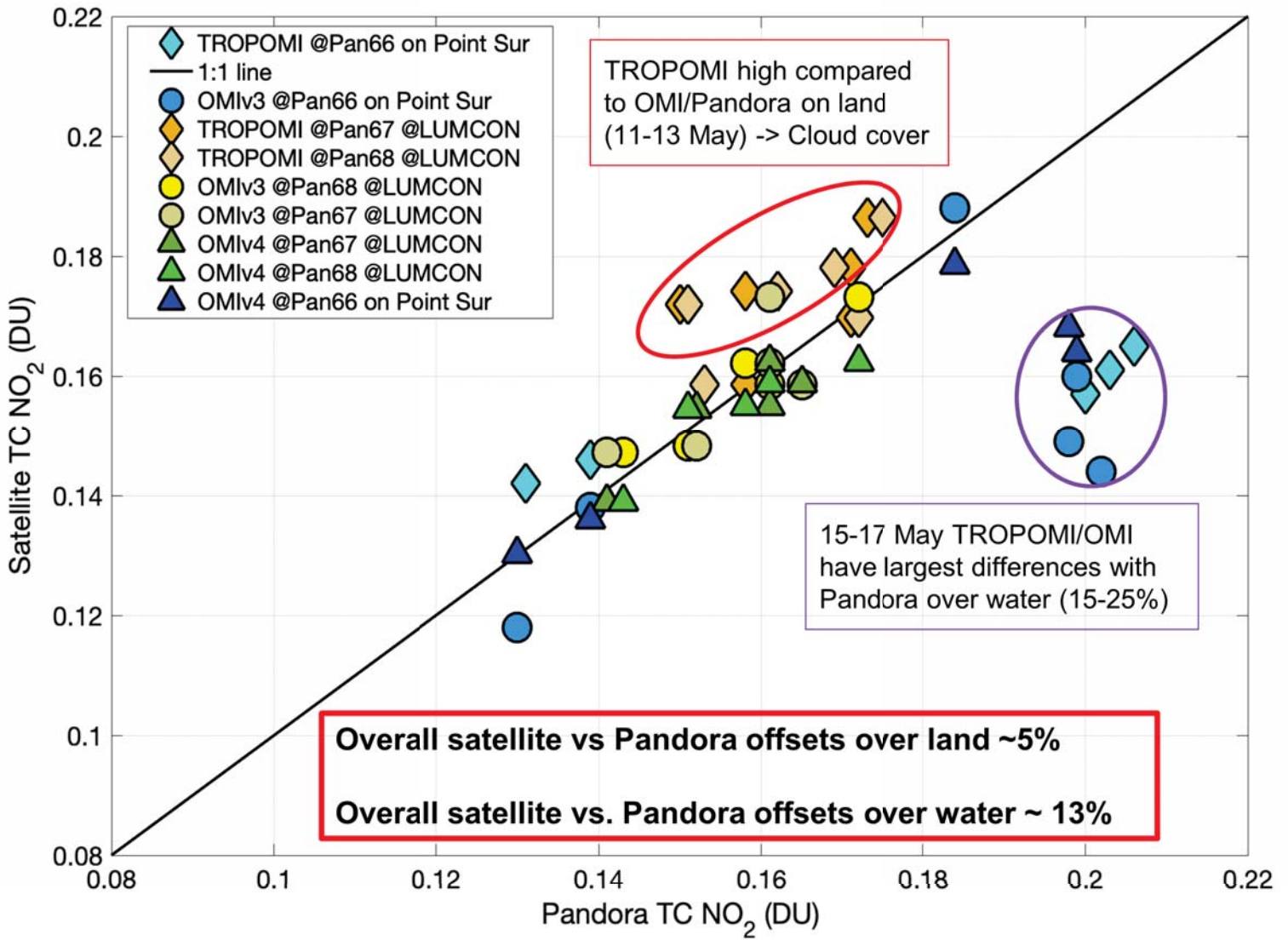


Figure 11.



Earth and Space Science

Supporting Information for

Two Air Quality Regimes in Total Column NO₂ over the Gulf of Mexico in May 2019: Shipboard and Satellite Views

Anne M. Thompson^{1,2}, Debra E. Kollonige^{1,3}, Ryan M. Stauffer¹, Alexander E. Kotsakis^{1,4}, Nader Abuhassan^{1,2}, Lok N. Lamsal^{1,2}, Robert J. Swap¹, Donald R. Blake⁵, Amy Townsend-Small⁶, Holli D. Wecht⁷

¹Earth Sciences Div., NASA/GSFC, Greenbelt, MD, USA

²University of Maryland Baltimore County, Baltimore, MD, USA

³Science Systems and Applications, Inc., Lanham, MD, USA

⁴ERT, Inc., Laurel, MD, USA

⁵Univ. California-Irvine, Dept. of Chemistry, Irvine, CA, USA

⁶Univ. of Cincinnati, Dept. of Geology and Geography, Cincinnati, OH, USA

⁷Bureau of Ocean Energy Management, Office of Environmental Programs, Sterling, VA, USA

Contents of this file

Figures S1 to S7

Tables S1 to S2

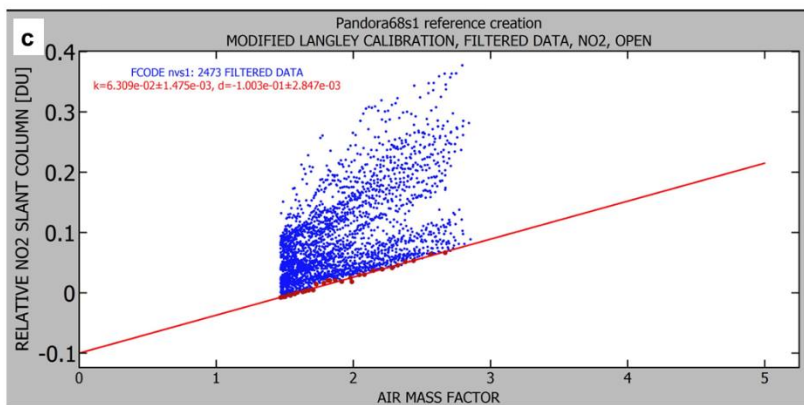
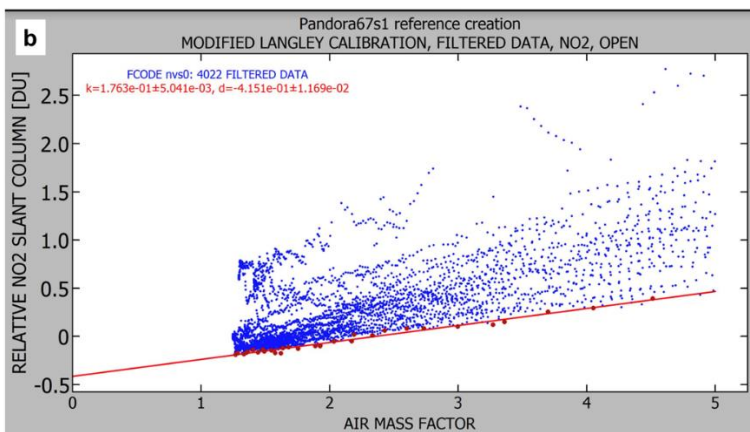
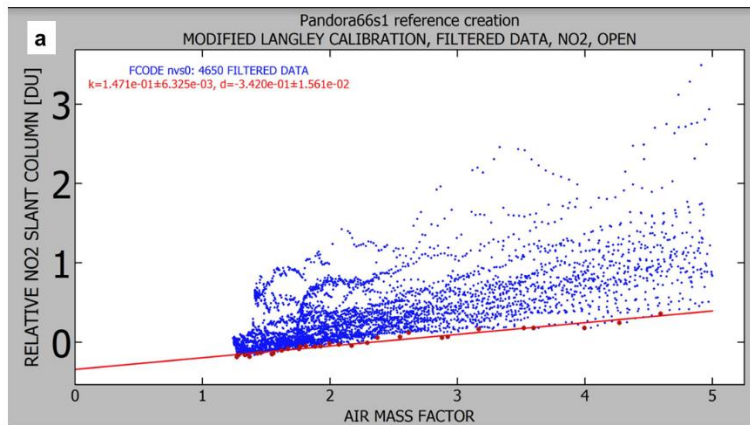


Figure S1. Screen shots of the spectra for Minimum Langley Extrapolation (MLE) using data collected between 17:55:00 UTC and 18:05:00 UTC on 20 April 2019 when all three Pandoras sampled clear skies and low tropospheric NO₂ amounts. Full statistics for calibration are based on 19 days of data at LUMCON, thus meeting the Luftblick Fiducial Reference criteria (*Luftblick*, 2022). (a) Pandora 66; (b) Pandora 67; (c) Pandora 68.

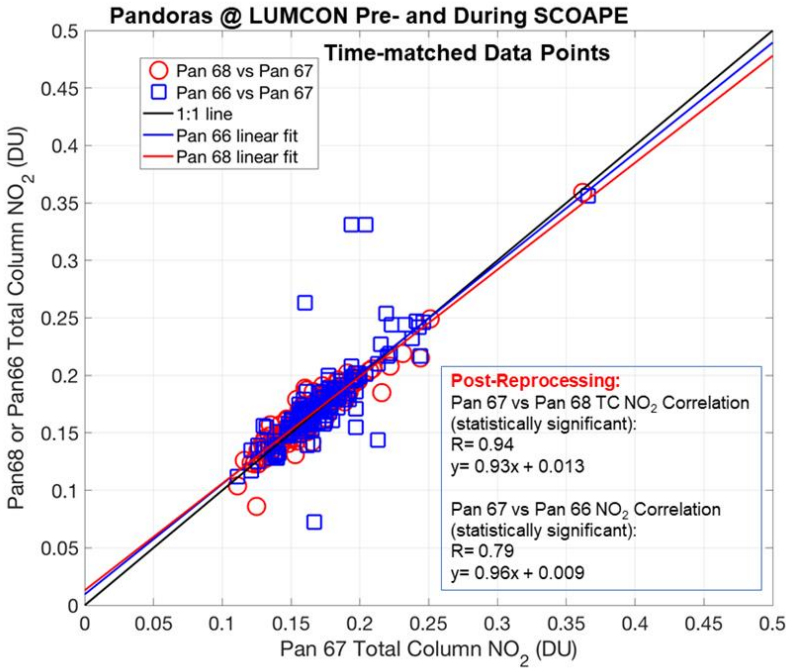


Figure S2. Time-matched data from Pandora 66 (blue squares) at LUMCON prior to cruise, 10 April to 8 May 2018. Comparison of Pandora 68 (red circles) referenced to Pandora 67 at LUMCON cover pre- and during the cruise, from 10 April–18 May 2019 ([data from NASA/LARC/SD/ASDC, 2022c](#)). Linear best-fit lines are blue and red, respectively, with 1:1 black line for reference.

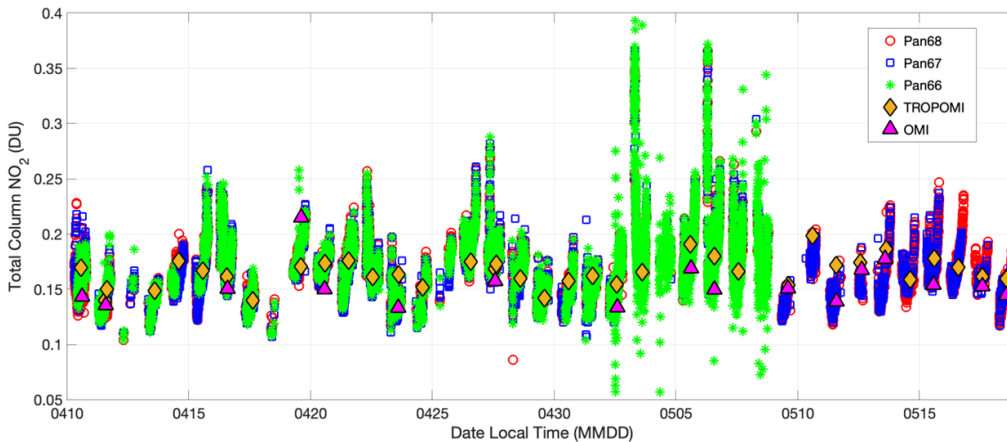


Figure S3. TC NO₂ as measured by Pandoras 66, 67, and 68 prior to the SCOAPE cruise ([data from NASA/LARC/SD/ASDC, 2022c](#)), from 10 April through 8 May with TROPOMI overpass readings- ([Copernicus Sentinel-5P, 2018](#)) in gold diamonds and OMI v4 data ([Krotkov et al., 2019](#)) in magenta triangles. After Pandora 66 was installed on the *R/V Point Sur* and only Pandoras 67 and 68 recorded TC NO₂ at LUMCON. A summary of satellite offsets from Pandoras appears in Tables S1 and S2.

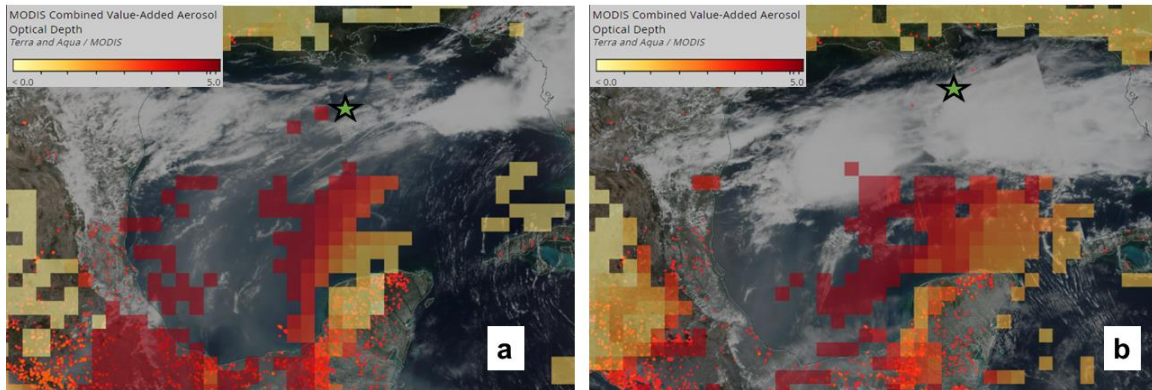


Figure S4. a) Moderate Resolution Imaging Spectrometer (MODIS) combined value-added aerosol optical depth ([Naval Research Laboratory and the University of North Dakota/MODIS Adaptive Processing System \(MODAPS\), 2017](#)) shows smoke and elevated aerosol counts from Mexican fires during SCOAPE campaign on 13 May (a) and 14 May 2019 [See [Duncan \(2020\)](#)].(b). SNPP VIIRS ([Schroeder and Giglio, 2017](#)) and MODIS ([Giglio and Justice, 2021](#)) thermal anomalies/fires counts are marked in red and orange dots, respectively. All satellite data taken from <https://worldview.earthdata.nasa.gov>. Green star is the approximate *R/V Point Sur* location at the time of Aqua satellite overpass.

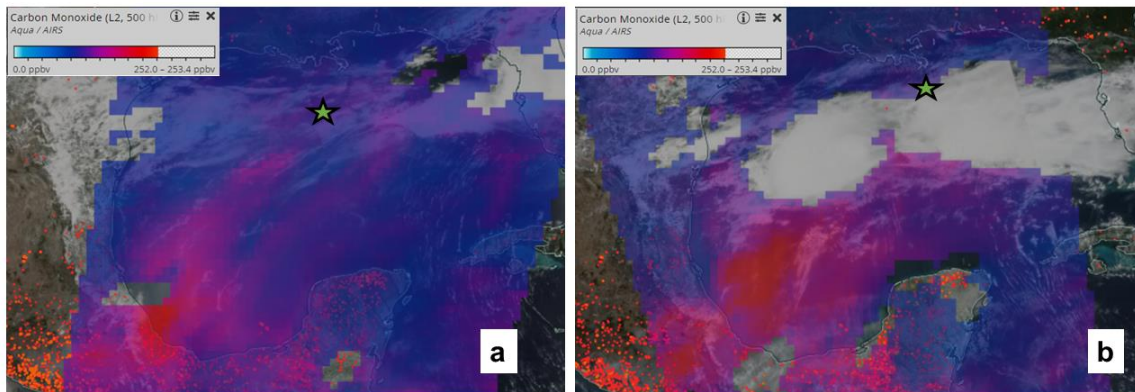


Figure S5. a) Atmospheric Infrared Sounder (AIRS) L2 carbon monoxide at 500 hPa ([AIRS Science Team/Joao Teixeira, 2013](#)) shows influence from Mexican fires on SCOAPE region on 13 May (a; night) and 14 May 2019 (b; day). SNPP VIIRS and MODIS thermal anomalies/fires counts are marked in red and orange dots, respectively. All satellite data taken from <https://worldview.earthdata.nasa.gov>. Green star is the approximate *R/V Point Sur* location at the time of Aqua satellite overpass.

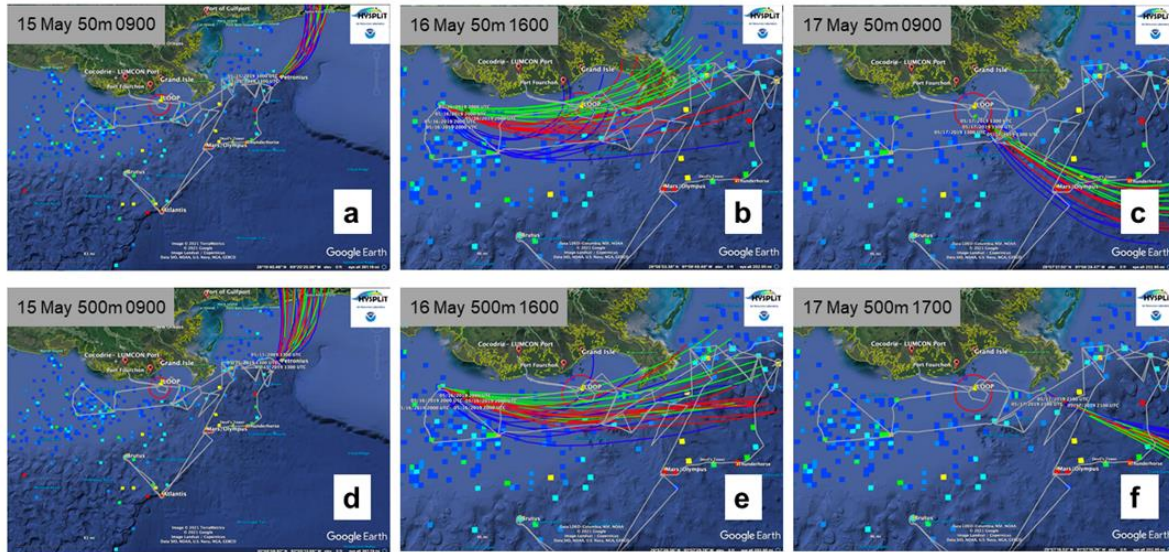


Figure S6. HYSPLIT 12-hour ensemble back trajectories ([Stein et al., 2015](#)) released at 50m (top panels; a-c) and 500m (lower panels; d-f) at the local times listed in each (15-17 May) and driven by the NCEP Global Data Assimilation System (GDAS) at 0.5° resolution. Colors of the trajectories denote change in ensemble trajectories' release time (every 3 hours over 12-hour period).

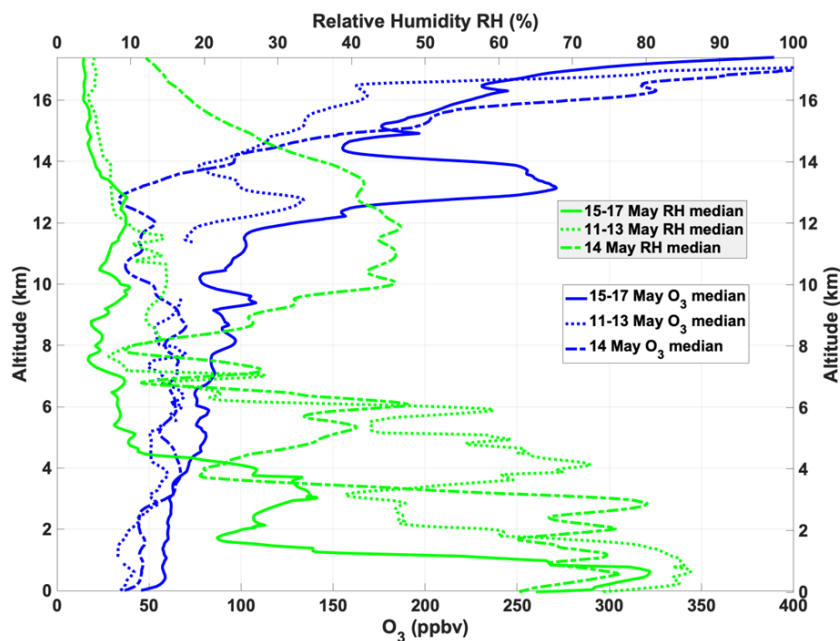


Figure S7. Median vertical profiles for ozone (blue lines) and relative humidity (green lines) from ozone and radiosondes launched from the *R/V Point Sur* during the cruise (11-17 May 2019). Dotted lines are for launches 11-13 May, dash-dot lines are for 14 May launches, and solid lines are for 15-17 May launches. [Data retrieved from NASA/LARC/SD/ASDC \(2022d\).](#)

Date	(P67 - TROPOMI) %	(P68 - TROPOMI) %	(P67 - OMI) %	(P68 - OMI) %
11 May 2019	-14.7	-13.9	1.5	2.9
12 May 2019	-10.3	-7.5	-1.6	-2.3
13 May 2019	-7.7	-6.5	-0.9	5.6
14 May 2019	-0.4	-3.7	---	---
15 May 2019	-4.2	-5.4	3.8	1.4
16 May 2019	0.7	1.3	---	---
17 May 2019	-0.4	-0.4	3.7	1.9

Table S1. Coastal satellite (TROPOMI and OMI v4) and Pandora (P67 and P68) comparisons during SCOAPE at Cocodrie, LA. Negative sign indicates that the satellite TC NO₂ value was higher than Pandora value.

Date	(P66 - TROPOMI) %	(P66 - OMI) %
11 May 2019	-5.0	2.2
12 May 2019	---	2.9
13 May 2019	-8.4	-0.2
15 May 2019	20.7	15.1
16 May 2019	21.5	---
17 May 2019	19.9	17.6

Table S2. Satellite (TROPOMI and OMI v4) and Pandora (P66) comparisons during SCOAPE over the R/V *Point Sur* locations.